

Review

Fissure Ridges: A Reappraisal of Faulting and Travertine Deposition (Travitonics)

Andrea Brogi ^{1,2,*} , Enrico Capezzuoli ³ , Volkan Karabacak ⁴ , Mehmet Cihat Alcicek ⁵ and Lianchao Luo ³¹ Department of Earth and Geoenvironmental Sciences, University of Bari, 70125 Bari, Italy² Institute of Geosciences and Earth Resources IGG-CNR, 56124 Pisa, Italy³ Department of Earth Sciences, University of Florence, 50121 Florence, Italy; enrico.capezzuoli@unifi.it (E.C.); lianchao.luo@unifi.it (L.L.)⁴ Department of Geological Engineering, Eskişehir Osmangazi University, Eskişehir 26040, Turkey; karabacak@ogu.edu.tr⁵ Department of Geology, University of Pamukkale, Denizli 20070, Turkey; alcicek@pau.edu.tr

* Correspondence: andrea.brogi@uniba.it

Abstract: The mechanical discontinuities in the upper crust (i.e., faults and related fractures) lead to the uprising of geothermal fluids to the Earth's surface. If fluids are enriched in Ca^{2+} and HCO_3^- , masses of CaCO_3 (i.e., travertine deposits) can form mainly due to the CO_2 leakage from the thermal waters. Among other things, fissure-ridge-type deposits are peculiar travertine bodies made of bedded carbonate that gently to steeply dip away from the apical part where a central fissure is located, corresponding to the fracture trace intersecting the substratum; these morphotectonic features are the most useful deposits for tectonic and paleoseismological investigation, as their development is contemporaneous with the activity of faults leading to the enhancement of permeability that serves to guarantee the circulation of fluids and their emergence. Therefore, the fissure ridge architecture sheds light on the interplay among fault activity, travertine deposition, and ridge evolution, providing key geo-chronologic constraints due to the fact that travertine can be dated by different radiometric methods. In recent years, studies dealing with travertine fissure ridges have been considerably improved to provide a large amount of information. In this paper, we report the state of the art of knowledge on this topic refining the literature data as well as adding original data, mainly focusing on the fissure ridge morphology, internal architecture, depositional facies, growth mechanisms, tectonic setting in which the fissure ridges develop, and advantages of using the fissure ridges for neotectonic and seismotectonic studies.



Citation: Brogi, A.; Capezzuoli, E.; Karabacak, V.; Alcicek, M.C.; Luo, L. Fissure Ridges: A Reappraisal of Faulting and Travertine Deposition (Travitonics). *Geosciences* **2021**, *11*, 278. <https://doi.org/10.3390/geosciences11070278>

Academic Editors: Alexander L. Strom and Jesus Martinez-Frias

Received: 17 May 2021

Accepted: 24 June 2021

Published: 30 June 2021

Publisher's Note: MDPI stays neutral with regard to jurisdictional claims in published maps and institutional affiliations.



Copyright: © 2021 by the authors. Licensee MDPI, Basel, Switzerland. This article is an open access article distributed under the terms and conditions of the Creative Commons Attribution (CC BY) license (<https://creativecommons.org/licenses/by/4.0/>).

Keywords: faulting; fissure ridge; active tectonics; travertine; paleoseismicity; geothermal areas

1. Introduction

In geothermal areas with carbonate reservoirs, thermal springs and travertine deposition have inseparably combined the effects of brittle deformation at shallow crustal levels ([1,2], and references therein). When the high pCO_2 hydrothermal fluids are flowing from a spring, CO_2 rapidly degases due to the lower atmospheric pCO_2 . This leads to oversaturation near the surface zone with respect to the calcite that therefore precipitates close to the spring, according to the well-known reaction: $2\text{HCO}_3^- + \text{Ca}^{2+} = \text{CaCO}_3 + \text{CO}_2 + \text{H}_2\text{O}$.

The high encrusting capacity of fluids at the surface and along the conduits at a relatively shallow depth implies that renewed permeability has to be guaranteed by tectonic activity in order to maintain the flowing of fluids. Curewitz and Karson [3] described two different primary mechanisms controlling the permeability's maintenance through time in fault zones permeated by hydrothermal fluids. These mechanisms guarantee the (i) dynamically or (ii) kinematically maintained permeability. The first case (i) implies faults that form and sustain the propagation of newly formed fractures in the rocks. In

this case, the fracture propagation at both tip-zones and wall-zones, linked to the stress concentration, and related thermal springs leads away from the main fault. The second case (ii) can be characterized by faults with intermittent movement that progressively re-open pre-existing filled fractures (i.e., veins) along the fault. This implies that thermal springs are active during periods of tectonic activity, following the seismic cycle of faults ([4], and references therein).

The neologism “travitonic” was introduced by Hancock, et al. [1], after suggestion by Prof. Robert Folk following the idea proposed by Muir-Wood [5], to fix the concept that travertine deposition and tectonic activity are inseparable processes. Among others [6,7], the paper by Hancock, et al. [1] opened a new perspective for neotectonic studies, shedding light on a new research approach based on decoding travertine deposits for tectonic analyses. Thus, since 1999 several researchers have applied the “travitonic” concept to seismotectonics and neotectonic investigation in geothermal areas around the world. Among the travertine bodies deposited from hydrothermal fluids discharged from thermal springs, fissure-ridge-type travertine deposits [8] have attracted most researchers, being the most prominent spring-related travertine deposit formed along the traces of brittle structures and therefore consolidating the strict link between travertine deposition and faulting [9,10]. It was later shown that the fissure ridge’s shape and internal architecture can reveal much about the geometry and kinematics of the main structure hidden by the travertine body [11].

Fissure ridges consist of elongated travertine masses with an apical fissure that follows the long axis of the body. Two symmetrical or asymmetrical walls made up of bedded travertine are typically dipping away from the central fissure (Figure 1). The internal part of the fissure is often cut by a network of sealed fractures, almost parallel to the long axis of the ridge, normally filled by banded Ca-carbonate (i.e., calcite and/or aragonite), almost parallel to the vein-walls (the so called “banded travertine” in [9,10]). These veins developed within the fault zone and represent conduits along which geothermal fluids move towards the surface [12,13]. Therefore, their analysis, in terms of geometry, age (using U/Th, U/Pb, and ^{14}C geochronology), and geochemical properties, provides information about the structural features and timing of the fault system, and on the fluid path from depth to surface [1,13–16]. Furthermore, travertine deposited in a fissure ridge is characterized by distinct petrographic and geochemical features preserving information on the parent fluids and ancient depositional conditions. The shape of the fissure ridge body depends on the flow rate, carbonate precipitation rate, and surface topography upon which deposition took place.

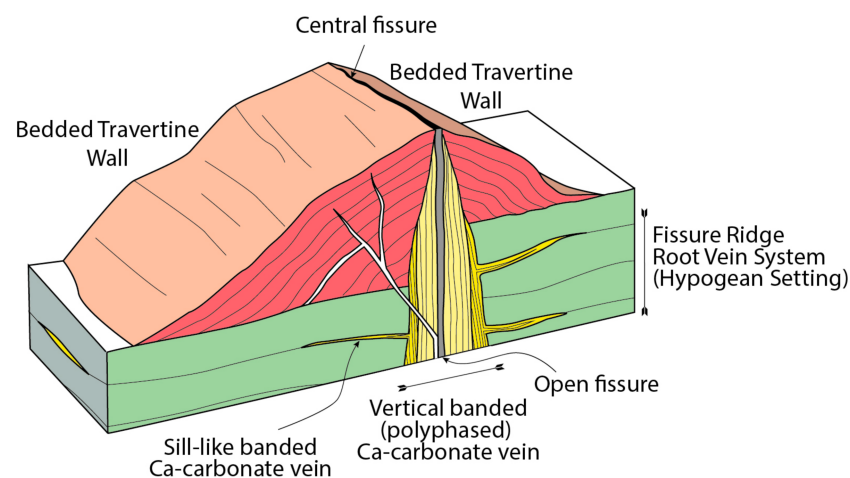


Figure 1. Diagram showing the anatomy of a fissure-ridge-type travertine deposit.

So, here below we describe the state of the art and updated knowledge on the fissure ridges, summarizing a large amount of information recently published on different fissure

ridges described in various geothermal areas of the world. In different sections, we deal with: (i) the fissure ridge morphology; (ii) travertine facies developing on the wall-slopes; (iii) growth mechanisms, (iv) banded Ca-carbonate vein features crossing the fissure ridge and its substratum; and (v) tectonic environments in which fissure ridges have been described to develop. We also aim to emphasize how these results update the potentiality of the fissure-ridge-type travertine deposits for neotectonics and seismotectonic investigations.

2. Fissure Ridge Morphology and Internal Architecture

Several fissure ridges have been described around the world by many authors, developed from the Mesozoic period [17,18] to the present [9,10,19–37]. Furthermore, the recent exploration of planets of the Solar System has also highlighted the possible existences of fissure-ridge-type travertine deposits and associated mounds in extra-terrestrial settings, as was “described” for Mars [38–41].

A fissure-ridge-type travertine deposit consists of a local relief caused by aligned thermal springs supplying the carbonate-rich waters (Figure 2a). Fissure ridges are described as straight or curvilinear in plain view and can be up to 2.5 km long, 400 m wide, and 25–30 m high. In section, a typical fissure ridge (Figure 2b) shows a triangular shape symmetrically or asymmetrically divided by a central fissure that separates the whole ridge into two walls. These latter are made of bedded carbonate (bedded travertine) dipping away from 5° to 90° from the central fissure running along its long axis. The central fissure corresponds in depth to a bundle of veins ranging from some millimeters to a few meters in width (Figure 2c), filled by vertical laminated palisade or fibrous calcite and/or aragonite (named “banded travertine” in [9,10]). In some cases, the apical fissure is open (Figure 2d), becoming subject to receiving detrital components deriving from the travertine walls (i.e., pieces of travertine with dimensions from cm to dm) along with remains of animal bones [42]. At the Mammoth Hot Spring area (United States), one fissure is even accessible, representing a constructional type of a cave (‘Devil’s Kitchen’; [43]).

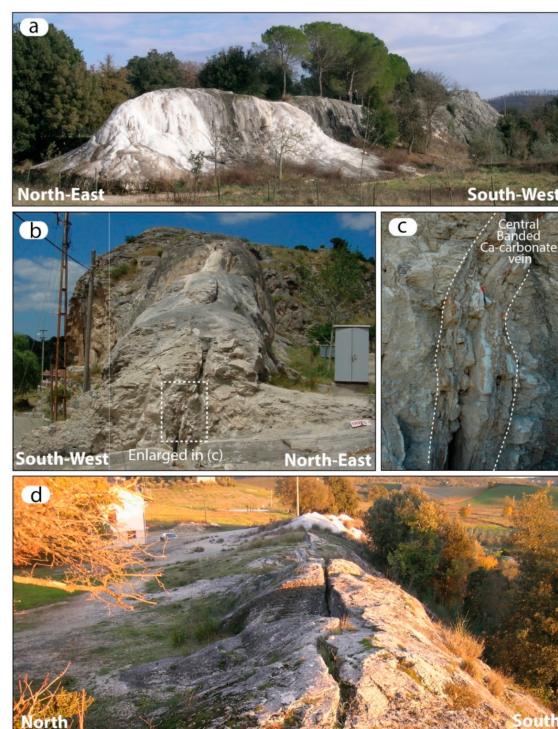


Figure 2. (a) General view of the Terme San Giovanni fissure ridge (Rapolano Terme, Italy); (b) Profile of a fissure ridge (Turkey) showing the central fissure partially filled by the banded Ca-carbonate vein; (c) Detail of the inset in b; (d) Fissure crossing the apical part of the ridge (Terme San Giovanni fissure ridge, Rapolano Terme, Italy).

The Ca-carbonate banded veins come upwards from the bedrock, which is hidden below the bedded travertine (Figure 3a–b). They have a sub-vertical geometry (Figure 3c) and develop on the walls of the fissure by upwelling thermal waters that afterwards flow out at the top of the ridge, promoting its progressive construction (Figure 3d,e). Ca-carbonate banded veins can also grow as sill-like structures and injection veins [11,15,31], giving rise to a more or less complex vein network (Figure 3f,g). Thus, the internal architecture of the ridge, its morphology (both in cross-section and in plain view), and the banded vein–bedded travertine relationships can reveal much about the fissure ridge’s evolution and brittle deformation affecting the substratum [11].

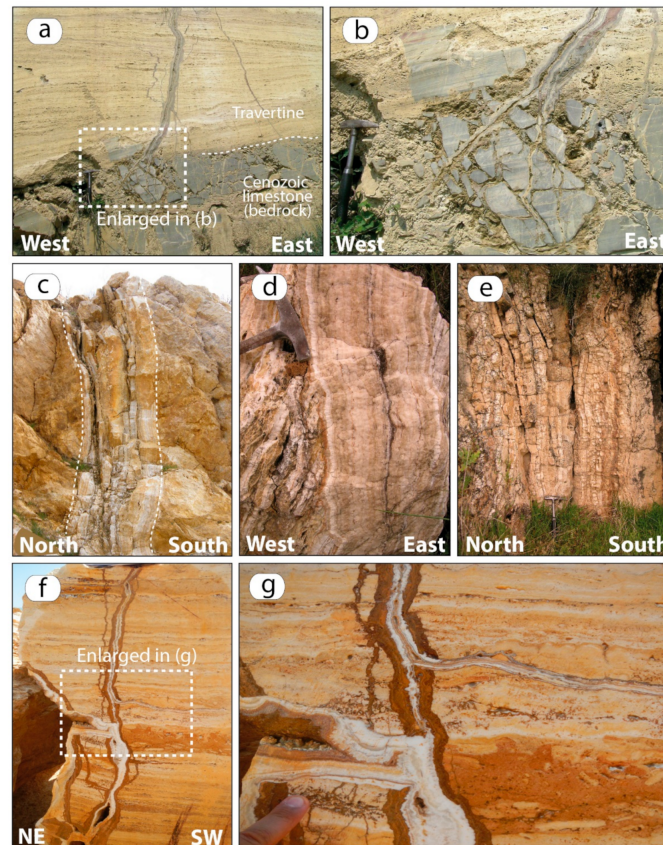


Figure 3. (a,b) Banded Ca-carbonate vein filling a fracture affecting travertine deposits and their substratum (from Bagno Vignoni, Italy); (c) An example of a vertical banded Ca-carbonate vein crossing travertine deposits (Denizli Basin, Turkey); (d) Cross-cutting relationships within a banded Ca-carbonate vein (Sant’Antimo quarry, Italy); (e) Multiple symmetrical banded Ca-carbonate veins (Denizli Basin, Turkey); (f,g) Christmas-tree-shape banded Ca-carbonate veins crossing travertine deposits (Akkoy, Turkey).

Fissure ridges are symmetric or asymmetric and, consequently, the opposite flanks forming the walls of bedded travertine are extremely variable in extension and dipping attitude. Fissure ridge end-members can be proposed on the basis of their symmetry/asymmetry (Figure 4): the symmetric ridge, developing on a horizontal substrate, has specular walls with respect to the central fissure and shows a right triangle shape; the asymmetric one, developing on a slope (i.e., a fault surface), mainly consists of only one wall that evolves in a slope travertine depositional system that grows mainly due to progradation. Examples are known in a plethora of areas, including: Pamukkale (Turkey), Mammoth Hot Spring (United States), and Bešeňová (Slovakia).

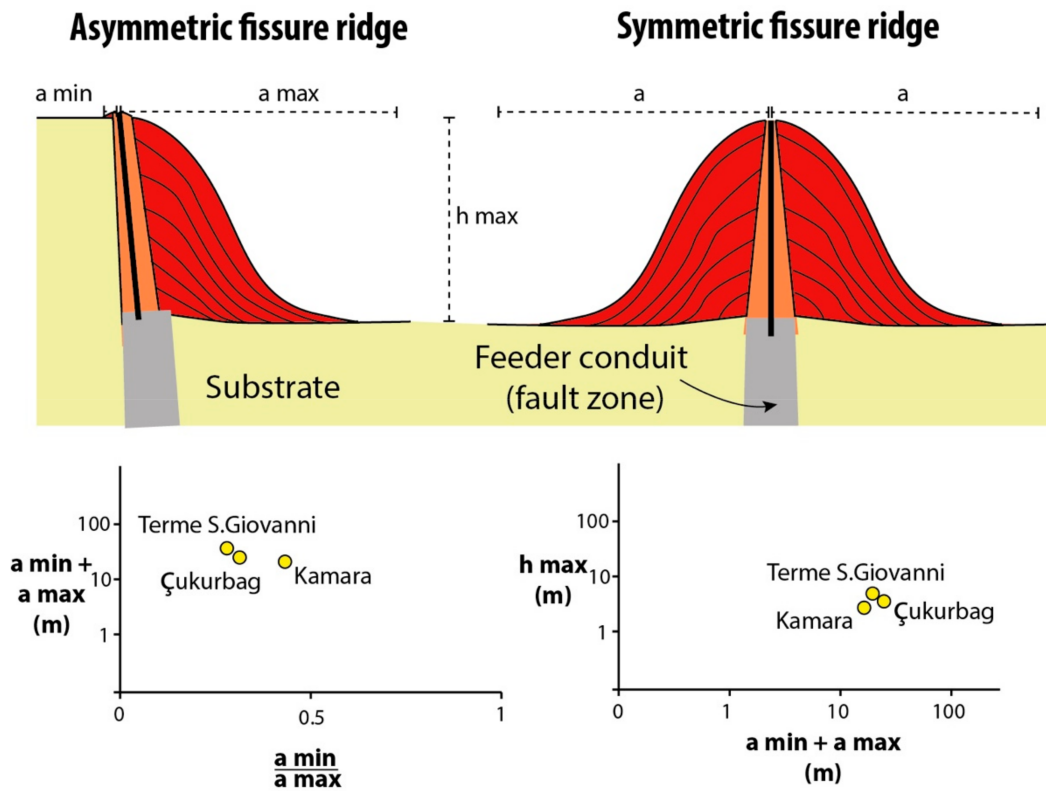


Figure 4. End-members of fissure-ridge-type travertine deposits and related diagrams.

We propose the term ‘fissured slope’ to indicate this end-member asymmetric fissure ridge (Figure 4). Geometrical parameters such as wall width (a_{max} and a_{min}) and maximum height can be plotted in cartesian diagrams to better quantify the ridge’s morphological shapes.

In some cases, the fissure running along the long axis of the ridge is subject to a rapid dilatation, in the order of a few fractions of a millimeter per year [44]. This fact can be interpreted as the result of two effects, possibly also combined: (i) a dilatation effect induced by the creeping movement of extensional faults, induced by their mechanical properties and geometry (Figure 5); and (ii) a fan-like expansion linked to localized subsidence of the substrate in response to the increasing weight of the travertine body giving rise to the gravitational collapse of the ridge.

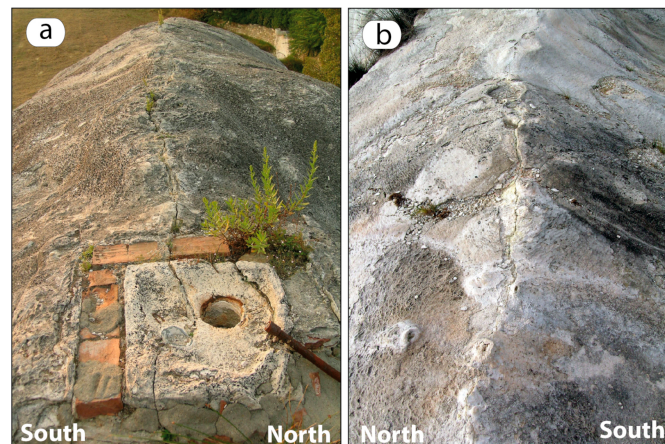


Figure 5. Incipient fissure affecting the apical part of the neoformed travertine deposit (Terme San Giovanni fissure ridge, Rapolano Terme, Italy). (a) the fissure is affecting artefact installed on the top in the 1950s. (b) the fissure is dissecting travertine deposited in recent times.

This second hypothesis has been proposed by some authors [32,33] to explain V-shape banded calcite veins crossing the topmost part of some fissure ridges. In their view, fissure ridges grew preferentially during warm and/or humid periods and were cut by banded Ca-carbonate veins during arid periods. So, paleoclimate oscillations rather than tectonics must have controlled the amount of fluid discharge influencing the opening of the feeding fractures by an increased pore pressure.

The height of the ridge is surely controlled by the fluid pressure (as discussed below), but their width and slope inclination can be the consequence of two combined effects: the fluid salinity and flowing velocity. If the salinity is high, the ridge tends to become tall and narrow; if the flowing velocity is high, the ridge tends to be low and wide at its base.

Finally, systems of fissure ridges can be distributed in an echelon formation, such as those from Gölemezli [20], Cambazlı [27], and Sıcakçermik [25,42], Turkey, suggesting fault arrays related to first-order fault zones, or in irregular shapes, therefore meaning that they contain few well-ordered tectonic structures.

3. Fissure Ridges vs. Mounds

Fissure-ridge- and mound-type deposits are end-members of tectonically driven morpho-tectonic features developing in the proximal zone of the travertine depositional system [45]. Fissure ridge development is favored along the trace of a fault affecting exposed bedrock [1], as deformation produces a continuous dilatational fracture along which fluids can uprise, forming aligned springs and associated ridge-shaped deposits (Figure 6a). Nevertheless, although aligned, the springs active on the ridge can produce localized cm- to dm-wide mound-type deposits (i.e., cones). Such evidence might be related to the fluid rate; if it is high (on the order of one liter per second, or more), water supersaturated with CaCO_3 flows laterally and produces localized fan slope depositional systems that can coalesce, contributing to an increase in the ridge wall (Figure 7). If the fluid rate is modest (in terms of less than a liter per second), travertine accumulates nearby the spring, forming a cone. These mound-shaped deposits are spaced from dm to m of each other along the apical part of the ridge (Figure 7). However, the progressive dilatation of the central fissure during the ridge's evolution dissects the cones, which therefore became inactive (Figure 7); as a consequence, a new spring activates nearby, forming a new cone that follows the trend of the fault (Figure 8).

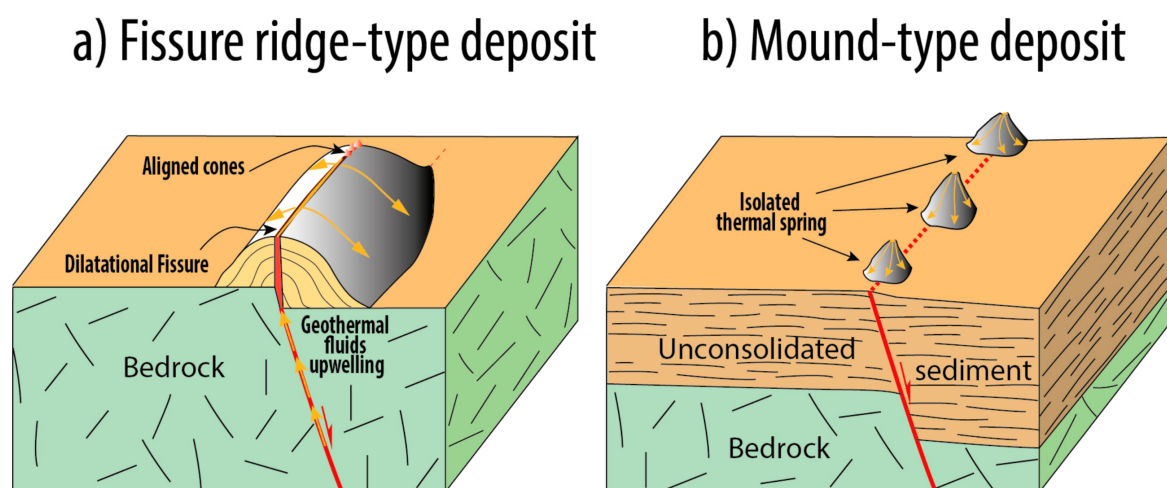


Figure 6. Diagram showing the geological setting favoring the formation of the fissure ridge (a) and mound-type (b) travertine deposits. See the text for more information.

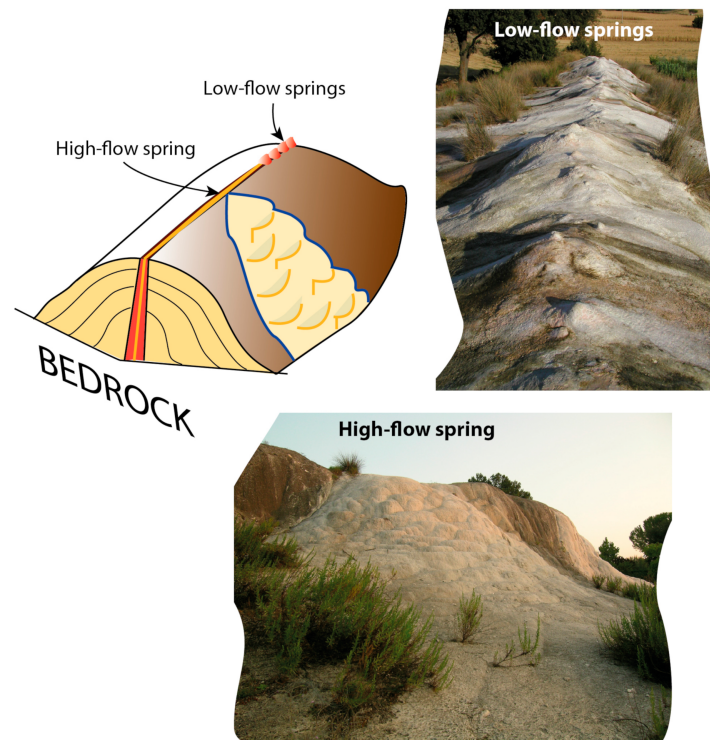


Figure 7. Diagram and photographs illustrating the formation of cones aligned along the fissure at the top of the ridge and the lateral slope depositional setting in relation to the flow spring. See the text for more information.

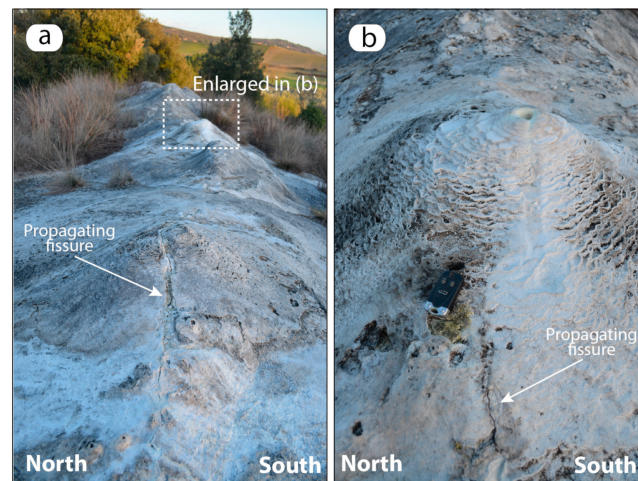


Figure 8. (a) Example of neoformal cones developed at the top of a fissure ridge cut by the propagating fissure (Terme San Giovanni fissure ridge, Rapolano Terme, Italy); (b) detail of the box indicated in (a).

Fissure ridge development is inhibited if the fault affects unconsolidated deposits. In this case, the fault-related permeability becomes extremely compartmentalized and fluids can emerge only in isolated points aligned along the fault trace (Figure 6b). If this is the case, isolated travertine mounds (cones, pinnacles, and towers) might develop (Figure 9). Mounds from Shiqiang [46] and Rongma, China [47] are good examples of this process.

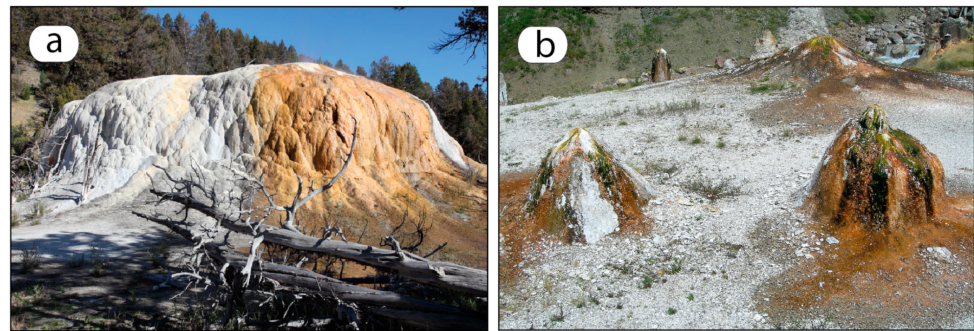


Figure 9. Photographs illustrating coalescing (a) and isolated mound-type deposits from the Yellowstone National Park (United States) (b).

Diameters of travertine mounds have normally been described to range from some decimeters to a few meters [8,46–51]; at the same time, their height can reach 14 m (e.g., “Liberty Cap” in Yellowstone National Park, United States [8]). The most impressive mound can be found in Iran (Zendané Soleyman) and is characterized by a height of ca. 100 m and a diameter of a few hundred meters [43].

It is obvious that any mound alignment occurs along the trace of the fracture supplying the geothermal fluids, as is the case for mounds from Hisaralan, Turkey [49] and lacustrine carbonate chimneys from Lake Abbé, Djibouti [52], still underlining the localized influence of fault/fracture-induced permeability on the control of the spring’s localization in unconsolidated sediments.

4. Facies

Deposition on the flank of the ridges is due to the physical/chemical changes in the thermal water flowing from the spring. CO_2 leakage and bacteria activity saturate the fluid in Ca and HCO_3 , thus inducing the Ca-carbonate (i.e., travertine) deposition. Different primary and secondary facies of travertine forms (epigean facies, Figure 10) depend on many factors, such as: (i) temperature maintenance, (ii) the flow rate, (iii) turbulence, (iv) the concentration of dissolved inorganic carbon, (v) pH, (vi) salinity, and (vii) the presence of Mg, Sr, and Mn. Biological factors, consisting of a distribution of benthic microbial biofilms, macro- and microphytes, and the slope gradient [53–56], can also influence the modality of carbonate deposition. They are also known as “bedded travertine” [9,10] and comprise sub-horizontal to very steep well-bedded and laminated lithofacies of variable lateral extent that pinch out from the central portion of the ridge. According to Gandin and Capezzuoli [57], they can be roughly described as generally characterized by an irregular alternation of laminae (or bands) of crust and detrital facies (Figure 10).

Crust facies can be subdivided into abiotic crystalline (characterized by dendritic/palisade macrocrystals and indicative of high-energy flows on steep slopes) [54] and microbially mediated crusts (or microbialites, characterized by microcrystalline carbonate/limemud entrapped by filaments or cohesively fixed by EPS mucilage). Crystalline facies are mostly located in the central, higher portion of the ridge, where they show highly inclined bedding and a compact fabric (Figure 11a). In the lower and distal smoother to sub-horizontal parts of the ridge, the lithofacies’ association shows a generally dominating porous fabric formed by laminar microbialites (bindstone, dendrolite, and crustone) locally associated with crystalline (typically foam and raft, Figure 11b,c), indicating slow flow on microterraced or gently undulating low-angle slopes (Figure 11d).

Granular facies are also typical of the distal portion, where autochthonous elements (intraclast, peloid, and coated grain) are transported and deposited, often together with allochthonous elements (skeletal/bioclasm and extraclast) due to energy dissipation (Figure 11e). Here, a transition to typical tufa fabrics can occur due to the progressive cooling of the thermal water or mixing with surface rainwater.

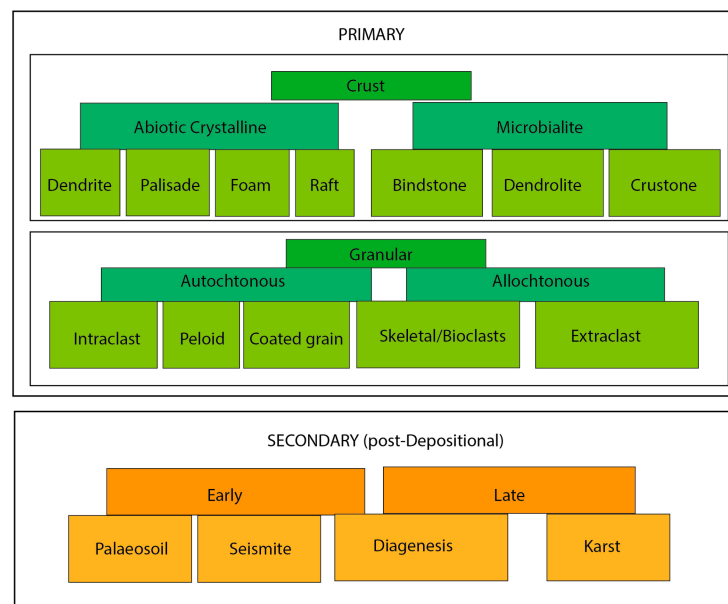


Figure 10. Diagram representing the main travertine facies associated with fissure ridges. See the text for their description.

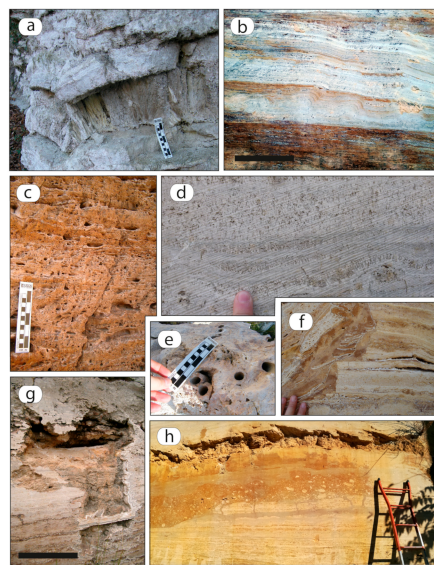


Figure 11. (a) Example of crystalline facies formed by dendritic, feather-like calcite crystals (Bagni San Filippo, Italy); (b) section of gently undulating, terraced, low-angle slopes with a dominant porous fabric formed by alternation of laminar microbialites (bindstone, dendrolite, and crustone) locally associated with crystalline ones (typically foam and raft) (Akkoy, Turkey) (black scale = about 40 cm); (c) example of highly porous laminar microbialites from a low-angle slope of Bagni San Filippo (Italy); (d) section of a small pool filled with alternation of crustones and microbialites (flowing water toward the left—Rapolano terme, Italy); (e) autochthonous encrusted skeletal grain (coated stems in the life position) often observed in a distal environment (Cambazlı, Turkey); (f) lateral passage from a fracture (on the left) and bedded travertine (alternation of crustones and microbialite—on the right). Notice the deformation of the bedded travertine and the secondary white cements developed in the opened voids (Akkoy, Turkey); (g) example of a karstic feature filled with secondary deposits (speleothems and terrigenous deposits) commonly developing in the late evolutionary stage (Bagno Vignoni, Italy) (black scale = about 70 cm); (h) example of seismically induced, soft sediment deformation structures from Rapolano Terme (Italy).

The rapid lateral juxtaposition or shifting of all these depositional facies [21,58] is a consequence of several microenvironments (waterfalls, pools, microterraced slopes, fans, and smooth slopes) rapidly developing one upon the other and determining undulating geometries (Figure 11b,f) along the slope gradient; note that these latter are deposition-related geometries that are not the consequence of syn-diagenetic folding (i.e., non-tectonic) [59]. The vertical accretion of the slope gradient causes diversion of the water flow that therefore can give rise to non-conformities where paleosoils and karst phenomena can develop (Figure 11f,g), bounding every single depositional unit. This early, secondary (affecting already-deposited sediments) feature can also be affected by seismically induced brittle [60,61] and soft sediment deformation structures (Figure 11h) [62] and an early diagenesis feature [63] that can be more impactful (together with karst) in the late evolution of the depositional system.

The deposition rate is generally very high-ranging, from some centimeters to a few meters per year [53], but its results are influenced by the climate (rainfall) and tectonics (earthquakes) in a short period.

5. Growth Mechanisms

Among the other causes (climate influencing the water table, CO₂ pressure fluctuations within the reservoir) [15,64], tectonic pulses, often accompanied by seismic shocks and ground shaking, are the main factors triggering the activation or reactivation of thermal springs in a fissure ridge [1,65]. In fact, earthquakes have a major role in renewing permeability by opening (or re-opening) fractures in rock masses. This process can be promoted in passive or active modes: (1) the passive mode implies a transient wave coming from a far epicenter, passing through the fault zone and associated fissure ridge, which reopens the sealed fractures; and (2) the active mode implies the (re-)activation of that fault along which fluids are flowing and the fissure ridge is developing. In this case, faults are active in areas with anomalous heat flow and geothermal gradients and therefore reasonably consist of aseismic structures or are characterized by a very scarce seismicity.

Some fissure ridges are the result of prolonged activity of the associated fault. The prolonged activity implies, in some cases, the deformation of the travertine walls (i.e., tilting, faulting, and fracturing) and the migration of the central fissure. The migration of the central fissure is the result of the natural evolution of the fault zone along which the fissure ridge is developing. In this case, a new fissure can develop in a ridge wall, producing a new fissure ridge overgrowing the older one. This produces non-conformities within the bedded travertine, in some cases with bedded travertine dipping in opposite ways (Figure 12).

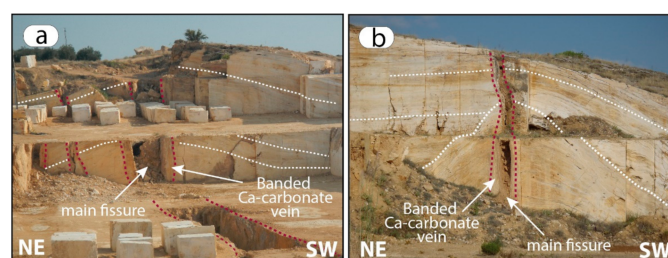


Figure 12. Different banded Ca-carbonate veins cutting travertine deposits migrating through time and giving rise to diachronous fissure ridges (Akkoy, Turkey). (a) panoramic view of the Ak-koy fissure ridge and the main fissure running at its top. (b) buried fissure ridge related to the progressive ridge migration.

Fault kinematics influence the geometry of the minor structures within the fault zone [66] with an impact on the fluid flow's localization. At the same time, the evolution of a fault zone can provide the migration of the main slip zone, for example jumping toward the hanging wall or foot wall, with direct effects on the final shape and internal architecture of the fissure ridge [11].

One part of the geometric and kinematics aspect, which varies on a case-by-case basis, is the over-pressured fluid that plays a primary role in determining the growth of a fissure ridge. In fact, thermal waters flowing at the surface can occur if (and only if) fluids have enough pressure. This can occur in particular hydrogeological settings where enough permeability and fluid pressure coexist. After a tectonic pulse, fluid within a fault zone that exceeds the hydrostatic pressure can flow after permeability is restored; the geothermal reservoir will then be hydraulically connected to the surface through re-opened fractures and fluids will run along the ridge, depositing travertine. In other cases, fluids can be compressed within the fault zone, therefore giving rise to sudden over-pressure, possibly producing hydrothermal eruptions and/or localized hydrofracturing [67].

As documented by various authors, abrupt co-seismic and post-seismic changes in water well levels [68–70] can be related to transient seismic waves, which are able to (i) promptly increase the pore pressure at depth [5,71] or (ii) trigger fluid pressure drops related to instantaneous permeability increases in the rock volumes [72,73]. In geothermal systems, earthquakes have been observed to perturb/trigger geyser eruptions [74] and cause mud-volcano development [75–77] or the abrupt activation of thermal springs [78–80]. Brogi and Capezzuoli [80] documented a clear relationship between earthquake-induced shaking and abrupt propagation of the fissure at the crest of a fissure ridge, permeability increases, and consequent (re-)activation of localized fluid discharge. This also demonstrates the notable impact of a low magnitude ($M=3.6$) seismic event produced by a seismogenic fault about 20–25 km away from the fissure ridge.

As previously mentioned, all these factors depend on the recharge capacity of the reservoir [81], in which the anthropogenic impact (in terms of fluids exploitation) plays a fundamental role. Climate factors, therefore, are important factors due to their influence on the amount of meteoric water infiltrating at depth and the CO_2 accumulation within the reservoir [15].

Thermal spring (re-)activation on a fissure ridge after a period of quiescence reasonably occurs at the less-elevated ridge end due to the fact that this part drops underneath the elevating water table level. The flow rate depends on the fluid pressure and does not allow the potentiometric surface to rise above the level of the spring. This is in apparent contradiction to the longitudinal profile of a fissure ridge, which shows a higher portion in the central part, implying the fact that the potentiometric surface must have risen to the top of the ridge and, therefore, must have exceeded the level of the spring at the lower end of the ridge.

The explanation of this apparent incongruence is related to the mechanism providing the growth cycle of a fissure ridge that develops after a single tectonic pulse. Tectonic activity gives rise to fault reactivation, which increases the permeability mainly at the tips of the fault segment, where new fractures can guarantee fault propagation (Figure 13a). At that time, over-pressured fluids trapped in the reservoir at depth are channeled along the new fractures, feeding thermal springs located at the extremities of the ridge, as these are the lowermost points available for resurgence owing to hydraulic pressure. Hydrothermal fluids leave the dissolved CO_2 , triggering the precipitation of travertine that accumulates at ridge margins. The progressive travertine deposition tends to seal the fractures and prevent continuous fluid discharge. Nevertheless, the destruction of permeability at the ridge margins favors the rise of the potentiometric surface, which will feed thermal springs located along the fissure and at a higher elevation (Figure 13b). The potentiometric surface will fluctuate or not depending on the fluid pressure condition. However, progressive travertine deposition and the related destruction of permeability result in the progressive migration of the thermal spring up to the top of the ridge, guaranteeing travertine deposition in the higher portion of the ridge (Figure 13c). The complete sealing of fractures feeding thermal springs inhibits travertine deposition and defines the end of the growth cycle. The following tectonic pulse(s), coupled with the availability of thermal water owing to favorable climatic conditions, can renew the permeability, offering the opportunity for repeated growth cycles and giving rise to progressive ridge development. In the case

of a tectonic pulse during an arid period, newly opened fractures are exposed to the air; therefore, banded travertine is prone to alteration by microbial activity and the evolution of the ridge is interrupted.

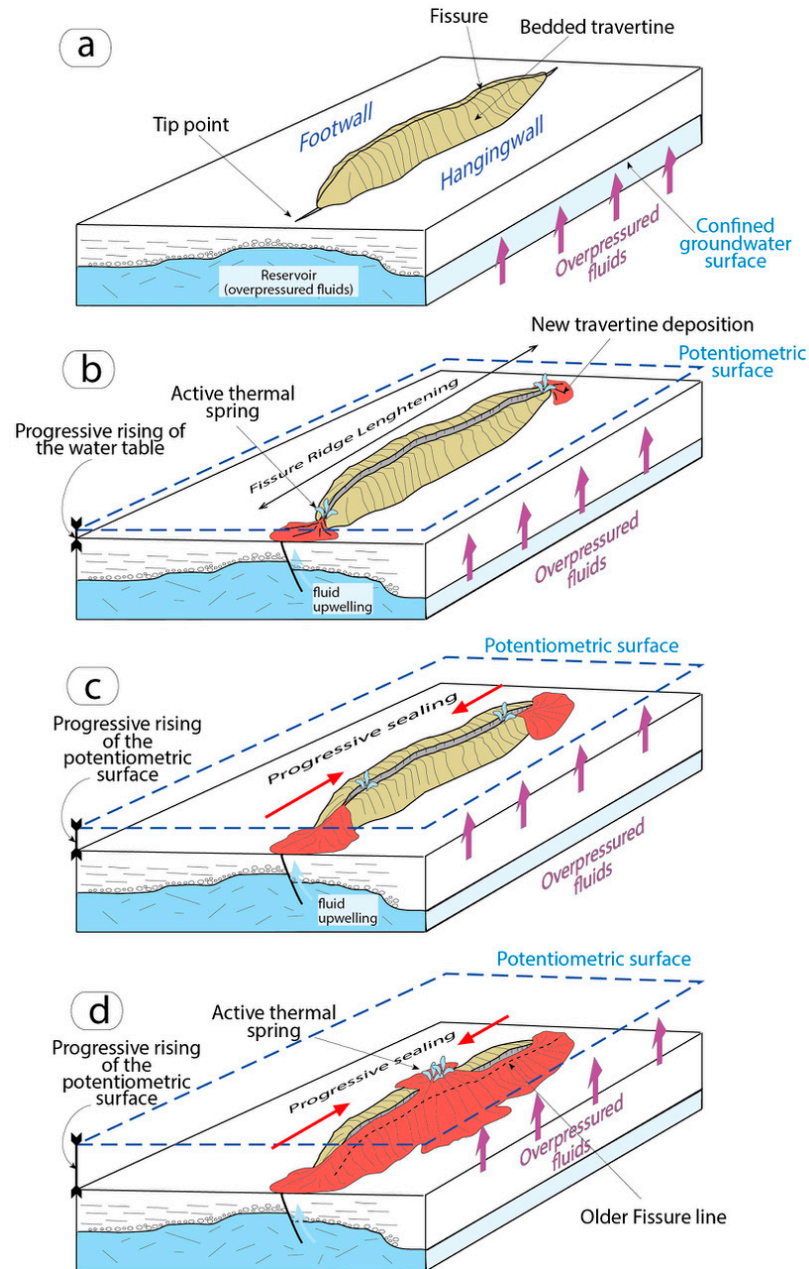


Figure 13. Schematic illustration of the conceptual mechanism controlling the development of a travertine fissure ridge based on the interplay between potentiometric surface level fluctuations and fracture sealing. (a) The fissure ridge during a tectonically quiescent period; at that time, the permeability is totally destroyed as a result of fracture sealing by Ca-carbonate veins. (b) After a tectonic pulse, the fault reactivates, re-opening previously sealed fractures and allowing for the over-pressured fluids to rise. Fluid discharges at the tip zones; here, flow is favored by the hydraulic gradient. (c,d) Progressive fluid flow seals the fractures at the ends of the ridge; consequently, the springs have to migrate toward the higher portions of the ridge up to the highest part (d). At that time, fracture sealing progressively inhibits fluid flow and the travertine deposition stops. A subsequent period of travertine deposition and fluid flow can be guaranteed by a new tectonic pulse (from [11], re-drawn).

6. Banded Ca-Carbonate Veins (Banded Travertine *Auct.*)

Banded Ca-carbonate veins fill most of the fissures crossing the fissure ridge and their substratum (Figures 2 and 14). Their development through time is due to progressive calcite/aragonite deposition by the flowing thermal waters. Banded veins have been described within the ridge substratum to be up to 12 m thick [13]. Banded veins within the fissure ridges, such as the Çukurbag fissure ridge [11] and the Ziga fissure ridge [82] in Turkey, are thinner, up to 4–6 m, and resemble well-laminated calcareous sinter as defined by Koban and Schweigert [83] and Flügel [84].

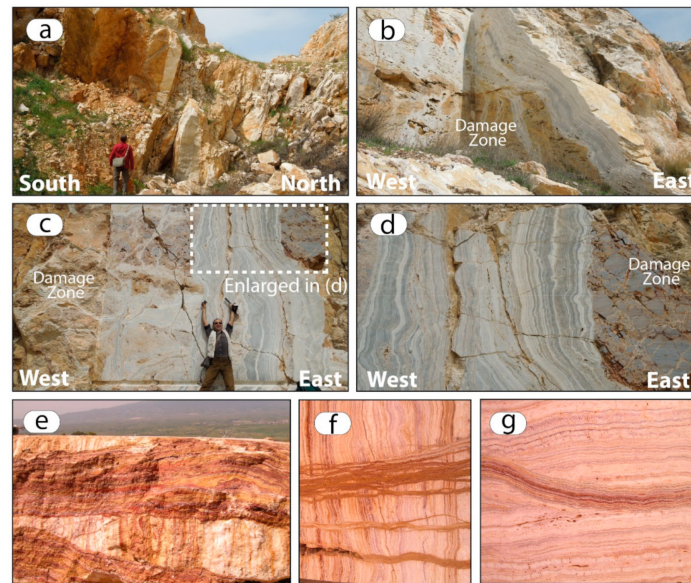


Figure 14. Banded Ca-carbonate veins filling the fracture network of the substratum of a fissure ridge and corresponding to the feeders of the spring. Examples from Golemezli (a–d) and Kamara area (e–g), Denizli Basin (Turkey).

Banded Ca-carbonate veins crossing the fissure ridges have been described by several authors from different geothermal areas [11,13,23,25,65,82,85–89]. These veins have a micro-laminated fabric (Figure 15) that, coupled with the syntaxial growth mechanism, indicates they are the consequence of repeated crack-and-seal events [90], thus implying iterate cycles of fracture opening followed by periods of carbonate deposition. In the root of the fissure ridge and in its substratum, Ca-carbonate banded veins fill a network of fractures that accompany the brittle deformation associated with the fault that feeds the thermal spring(s) from which the fissure ridge developed (Figure 1). This results in a hypogean setting [2,9,14,15,35,91–95] characterized by vertical or sub-horizontal (sill-like) mutually crosscutting bundles of cm-thick, onyx-like crystalline calcite/aragonite veins exhibiting sharp contacts with host rocks (Figure 14). Their syn-tectonic formation is evidenced by (i) displacement of pre-existing veins, (ii) the presence of interbedded, intraclastic cemented breccia deriving from fracturing of previous veins, the occurrence of lithons of the hosting rocks, (iv) mechanical striations of the previous veins, and (v) shear structures [2,13].

The texture of the Ca-carbonate banded veins is similar for both veins crossing the fissure ridge and its substratum. The multiphase vein infill is generally organized into finely laminated crystalline calcite/aragonite bands (Figure 15) that are sometimes multiple colors depending on the water's geochemistry, with the typical primary fabric formed by alternating accretion/overgrowth of elongated, blocky crystals and microsparite–micrite bands. They are interpreted as originating from the vein walls in phreatic conditions and characterized by moderate CO₂ degassing (Type A) or intense degassing likely related to a rapid re-opening of fractures after a period of clogging (Type B). Accessory fabrics are represented by dendritic, tree-shaped crystalline levels [36,96–98] and bituminous/organic

veneers coating the crystal terminations and representing short-lived situations in phreatic conditions without crystalline precipitation.

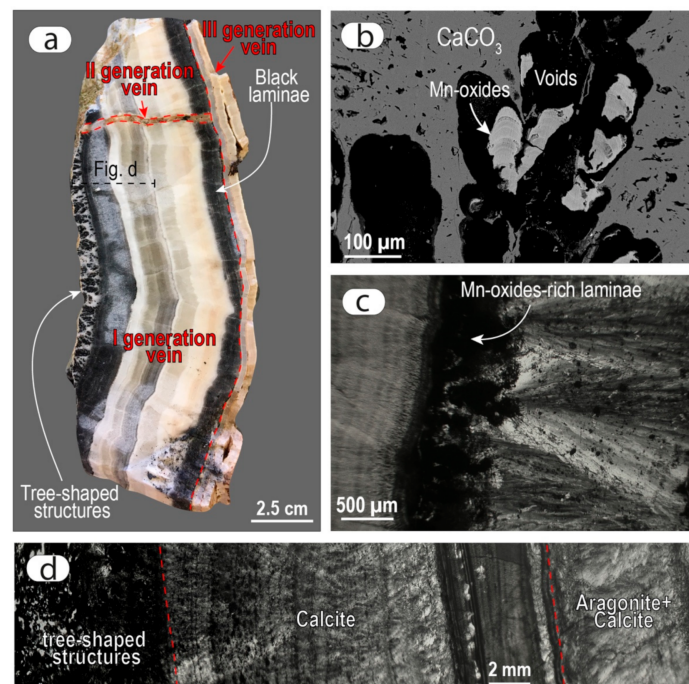


Figure 15. (a) Example of a banded Ca-carbonate vein composed by three superimposed veins; (b) SEM image of the Mn-oxide lamina characterized by a subrounded shape of different shades of gray. Brighter gray suggests a higher Mn-oxide concentration. (c) Micrograph (crossed polars) showing detail of Mn-rich laminae. (d) Micrograph (crossed polars) of a PAM1 sample showing bands made up of calcite and (Sr)-aragonite (from [36], re-drawn).

The deposition of aragonite is favored by a rapid precipitation rate, a high $p\text{CO}_2$ level, and an elevated Mg/Ca level [99]. Owing to the rapid precipitation rate, the banded travertine veins can minutely record deposition that occurred during short time spans and are represented by thick crystalline layers. The presence of a biological alteration at the top of many laminae suggests that fracture walls can periodically be exposed to the air, and so the vein surface was altered by biological activity. This implies that, in some cases, the opening of a vein was not accompanied by instantaneous water flow. In some cases, debris and fragments of travertine coming from the wall ridge can be found within the veins, thus underlining the existence of periods of quiescence and non-deposition paraconformity (hiatus).

In different tectonic domains, the growth rates of individual veins were calculated to be in the range between 0.01 and 0.11 mm/year without taking into consideration the paraconformity (hiatus) between the alternating bands [8,23,25,32,65].

Moreover, radiometric dating of some banded travertine veins crossing the Çukurbağ fissure ridge [15] indicates that a single band, that shows no growth discontinuities (hiatuses), of about 40 cm in thickness is representative of about 400 years. In line with the previous studies, therefore, Karabacak, et al. [65] infer that the time span of precipitation of a 1 cm thick Ca-carbonate band ranges between 20 and 300 years.

The intimate association of banded Ca-carbonate veins with seismicity and their triggering of the mobilization of CO_2 -rich fluids have been extensively demonstrated [15,23,65,92,100]. In this sense, banded travertine vein networks most probably represent the best near-surface product of CO_2 -driven hydrothermal eruptions in seismically active zones [14,15,65].

Karabacak, et al. [65] sum up the precipitation of Ca-carbonate bands in three descriptive periods in relation to seismicity (Figure 16): (1) a co-seismic period, which is represented by the expulsion of abundant depressurized/supersaturated hot water, re-

sulting in the rapid precipitation of whitish microcrystalline carbonate as a single band on both walls of the fracture; (2) a post-seismic period, which involves the continuation of saturated fluid discharge with a relatively slow flow rate and the light-transparent macrocrystalline calcite bands precipitating with slow degassing rates until the fracture is completely plugged; and (3) an inter-seismic period in which stagnant flow conditions mean that the lack of carbonate precipitation forms a hiatus with the former carbonate band. Thus, microcrystalline carbonate crystals (i.e., the nearest location of the band to the fracture wall) provide a great opportunity to directly date the event horizons of each individual period of seismic unrest.

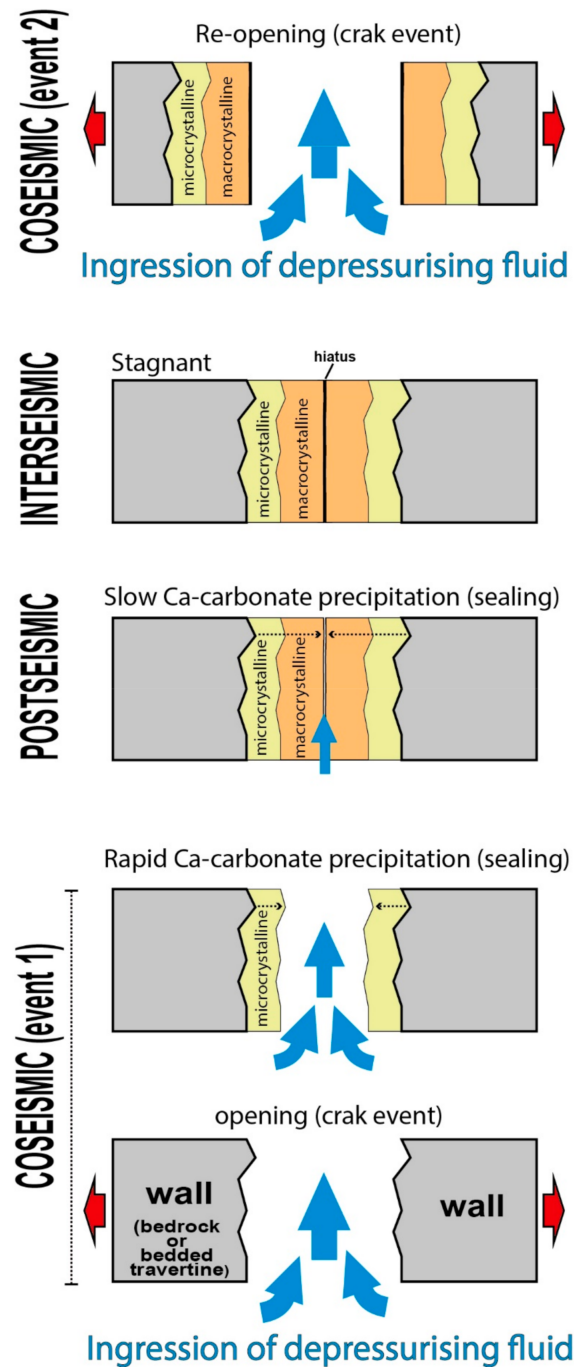


Figure 16. Diagram showing the conceptual mechanism forming the banded Ca-carbonate veins during a seismic cycle. See the text for more details.

Uysal, et al. [101] document trace element and O isotope data of the vein system interpreted as associated with seismic cycles involving fluids with different trace element compositions and CO₂ contents. They reached the same conclusion: initial carbonate precipitation occurred during a single seismic cycle due to the CO₂ degassing from the fluid. This was followed by carbonate precipitation from the remaining water, which was relatively impure with higher trace element contents. U-series dating in conjunction with the geochemistry of carbonate veins can therefore offer the possibility to constrain ages for both seismic and inter-seismic events.

Additional information from Matera, et al. [36] refers to the deposition of aragonite bands during co-seismic periods. Aragonite deposition instead of calcite deposition is controlled by different factors: (i) the high temperature of water [102–104]; and (ii) the high content of Mg [105,106] and Sr [107] in the hydrothermal fluid. Nevertheless, aragonite deposition is also controlled by the rate of CO₂ degassing [102] and, thus, the partial pressure of CO₂ [108] induces a high level of supersaturation and an increase in pH, both triggering the rapid deposition of aragonite.

Pulses of tectonic activity can therefore trigger a high CO₂ degassing rate and a partial pressure fluctuation, causing disequilibrium due to the kinetic effect, with a sensible impact on the signature of stable isotopes. Aragonite, in fact, displays a larger $\delta^{13}\text{C}$ variation than $\delta^{18}\text{O}$. Aragonite deposition occurs under disequilibrium conditions, isotopically light carbon dioxide preferentially escapes, and, as a consequence, the ¹³C and ¹⁸O contents when depositing CaCO₃ increase in the same direction [14,15,36]. In contrast, isotope values of calcite crystals during inter-seismic periods normally suggest that the isotopic composition of fluids remains constant during the formation of calcite crystals, and (possibly) that crystals form under isotopic equilibrium. Tree-shaped black structures containing manganese dioxides, which are based on [MnO₆] octahedra units linked in chains to form a framework structure containing monodimensional tunnels with specific sizes, can also develop during the inter-seismic periods [36]. The black tree-shaped structures mainly consist of todorokite and possibly cryptomelane and/or hollandite and are strictly associated with bacterial activity that promotes the precipitation of Mn-oxides. Precipitation produces aggregates with a high Mn concentration (Mn-oxides), even from water with a low Mn²⁺ concentration (in the parts per million range) [97]. This process is very likely promoted by pH changes that strongly depend on temperature and CO₂ degassing rate variations. Values of pH above 5 and oxidizing environments promote the precipitation of Mn-oxides [109]. Tree-shaped Mn-oxide structures are, therefore, indicative of a low-temperature fluid depleted in CO₂ occurring after rapid CO₂ degassing and mixed with meteoric waters, therefore suggesting a phase of transition after a fast CO₂ degassing event during which hydrothermal waters mix with more surficial ones, causing a temperature decrease.

Uysal, et al. [110] suppose that the CO₂-driven hydrothermal eruption process may be related to global and regional dry periods, especially during the late Quaternary. Moreover, Karabacak, et al. [89] found out that the oxygen isotope records of Ca-carbonate bands correlate well with those of marine and sub-terranean carbonates.

In sum, some authors [9,33,62,110,111] relate the banded Ca-carbonate veins and travertine deposition to paleoclimate effects. However, tectonic activity is the most fundamental factor determining fracture opening and related permeability in the rock masses, which are indispensable to promoting the hydraulic connection of the reservoir to the surface. Accordingly, fissure ridges are the most significant travertine masses in tectonic investigations, especially when both the banded and bedded travertines are exposed.

7. Tectonic Settings Favoring Fissure Ridge Development

Extensive documentation of the tectonic environments in which fissure ridges develop has been published in recent years, and it has been highlighted that fissure-ridge-type travertine deposits are associated with different classes of active faults as reported in Table 1.

Table 1. Reported fissure ridges in the world.

Locality	Fissure Ridge Name	References	
Italy	Terme San Giovanni	[26,80]	
	Semproniano	[35,95]	
	Bagni San Filippo	[110]	
	Rapolano Terme	[21,44,58,67,112–115]	
	Iano	[36]	
	Bagno Vignoni	[116]	
	Tivoli	[6,32,33]	
Turkey	Bal (Balkayası) (Caberkamara, Gediz basin)	[20]	
	Canbazlı (Ahmetli, Gediz basin)	[27,29]	
	Çukurbag (Denizli)	[9–11,31,33,117]	
	Çukurbag “little-sister” (Denizli)	[118]	
	Kamara (Denizli)	[2,20,33]	
	Akköy (Denizli) (Karakaya and Hanife hills)	[20,117]	
	Gölemezli (Denizli)	[13,119]	
	“Fissures at Pamukkale plateau”	[9,10,19]	
	Denizli basin	[1,14,15,23,31,101,110,120]	
	Çamlık (Başkale, Van)	[121]	
	Akhüyük (Ereğli, Konya)	[122]	
	Ortaköy (Sivas)	[123]	
	Reşadiye (Tokat)	[65,124,125]	
	Sıcak Çermik Delikkaya, Sarıkaya (Sivas) (Sivas)	[25,125,126]	
	Akkaya (Eskipazar, Karabük)	[88]	
	Kayabaşı, Kuşdili (Kırşehir)	[22,28]	
	Hacılar, Elmalı (Bingöl); Baltaşı, Karakocan (Elazığ)	[127,128]	
	Balkaya, Sarıhıdır (Avanos, Nevşehir)	[89]	
	Ziga (Ihlara, Aksaray)	[82,129]	
	Yeniçağ, Çiğdem, Üçtepeliler, Çepni (Bolu)	[85]	
	Tripolis (Barbaros Quarry)	[2]	
	Yaprakhisar-Ziga	[130]	
	Ereğli (Konya)	[122,131]	
	Balkaya, Sarıhıdır (Avanos, Nevşehir)	[89]	
	Bolu and Yenicag Basins	[65,85,124,132]	
	United States of America	Mammoth Hot Springs (Wyoming) and Bridgeport (California)	[8,30]
		Utah	[16,93]
Rio Grande		[133]	
Hungary	Sutto	[134]	
	Tata	[135]	
Slovakia	Drevenik	[60,61]	
Tunisia	Gafsa	[136]	
Iran	Ab-e Ask	[137–139]	
	Lake Urmia	[140]	
	Qorveh-Takab	[141]	
	Sahand Volcano	[142]	
	Sanandaj-Sirjan zone	[37]	
Argentina	Macizo del Deseado	[143]	
	Cerro Negro	[17]	
Kenya	TurkanaBasin	[144]	
Chile	Barrancas Blancas	[145]	
Scandinavia	Pechenga Greenstone belt	[146]	
Germany	Bottingen and Laichingen	[147]	
Japan	Futamata hot spring	[148]	
Morocco	Tafilalet	[149]	

De Filippis and Billi [31] invoke the fundamental role of pre-existing fracture patterns in both travertine masses and their bedrock, or the gravitational collapse of the travertine walls, in controlling travertine deposition due to the fluid pressure improvement. Therefore, in their view, tectonic activity plays a secondary role in the development of the fissure ridges, whereas climate, gravitational, and morphological processes are considered to be primary factors. However, in most cases, travertine fissure ridges have been intimately linked to faults. Normal fault and strike–slip fault systems, or both co-existing in a common stress field, have been described in many places and are considered to be able to control travertine deposition, especially in Italy and Turkey (Table 1).

However, the development of fissure ridges has been described in a wide range of tectonic settings as classified below:

1. along traces of normal faults [19,26,131,133,140];
2. on the hanging wall of a normal fault [130];
3. in step-over zones between adjacent normal fault segments (i.e., relay-ramps) [20,27,29,119];
4. in a shear zone [25];
5. in the damage zones or splay zones of strike–slip faults [88,121];
6. in the distributed deformation zone across strike–slip faults [65,124,125];
7. along strike–slip fault segments [11,85,122,127,136];
8. in releasing step-over zones linking strike–slip faults [85];
9. in restraining step-over zones linking strike–slip faults [85,128];
10. the deformation zone of a thrust fault [123];
11. at the tip of regional fault zones [112];
12. on extensional fractures aligned tangentially to the volcanic conduits [82,89,129].

8. Advantages of Using Fissure Ridges for Neotectonic and Seismotectonic Studies

A major advantage of investigating fissure-ridge-type deposits is that they are intimately related to a fault that produced (actively or passively, see the previous section) permeability at the time of its development. Permeability maintenance might be related to episodes of increased earthquake faulting following the suggestion of Brogi, et al. [2, and references therein] that, during earthquakes, co-seismic strain will re-open cracks previously sealed by Ca-carbonate precipitation, thus expelling geothermal fluids from the reservoir to the surface. A new cycle of carbonate deposition occurs along the wall slopes or within neoformal fractures (i.e., banded Ca-carbonate veins) and each Ca-carbonate band corresponds to a permeability enhancement period and possibly to a tectonic pulse [1,5,150].

This background, coupled with the fact that Ca-carbonate can be dated by the U-series method and the ^{14}C method and integrated by palaeomagnetic signatures [34], allows us to consider fissure-ridge-type travertine deposits as favorable (almost unique) deposits for neotectonic and seismotectonic studies.

Information from paleoseismicity is also possible; in fact, our understanding of the recurrence of earthquakes at timescales longer than instrumental and historical records can provide considerable advantages through U-Th dating of Ca-banded calcite veins forming in fissure-ridge-type travertine deposits, which are able to record more than 400 ka of an earthquake's history [100].

In a fissure ridge along the North Anatolian Fault, this hypothesis was tested directly for the first time with robust historical earthquake records and paleoseismic data [65]. The results suggest that the events recorded in Ca-carbonate veins indicate an epicenter with a distance of <200 km and high-intensity ($I > VI$) paleoearthquakes; thus, this tool has advantages over traditional paleoseismological methods for the understanding of long-term earthquake behavior. In this view, it should be possible to use age determination to reconstruct the seismicity and its recurrence [23,65,100], the fault dilatation rate [82], the age of a fault [36,65,112,116], an assessment of the slip rate [124], and relationships between faulting and fluid properties in geothermal fields [2,13,35,86,94,132,151–154].

9. Concluding Remarks and Neotectonics/Seismotectonics Implications

Travertine is a useful proxy for the reconstruction of the fluid features in geothermal areas. The presence of travertine, as well as the associated Ca-carbonate vein network in the substratum, suggests a widespread hydrothermal circulation within a carbonate reservoir at depth.

Fissure ridge occurrences and aligned mounds indicate that fluid resurgence is (or was) tectonically controlled by faults and/or fractures.

Analyses of a fissure ridge can reveal much about the tectonic regime that favored (or is favoring) the maintenance of permeability and, therefore, the fluid flow. Isotopic analyses and determination of the age of the bedded travertine forming the ridge and each band forming the Ca-carbonate veins crossing the ridge and the substratum have a twofold fallout: they allow us to date the main tectonic pulses, helping us to reconstruct the paleoseismic history of the area, and the climate fluctuations/fluid–rock interactions generated by the geothermal fluids.

The dilatation of the central fissure and the age and thickness of the banded veins indicate the deformation rate.

Finally, the growth of fissure-ridge-type travertine deposits with active thermal springs implies the existence of active faults.

Author Contributions: Conceptualization, A.B.; methodology, A.B.; E.C.; V.K., M.C.A. and L.L.; software, A.B.; E.C.; V.K., M.C.A. and L.L.; formal analysis, A.B.; E.C.; V.K., M.C.A. and L.L.; investigation, A.B.; E.C.; V.K., M.C.A. and L.L.; data curation, A.B.; E.C.; V.K., M.C.A. and L.L.; writing—original draft preparation, A.B.; writing—review and editing, A.B.; E.C.; V.K., M.C.A. and L.L.; supervision, A.B. All authors have read and agreed to the published version of the manuscript.

Funding: This research received no external funding.

Informed Consent Statement: Not applicable.

Data Availability Statement: Not applicable.

Acknowledgments: We are grateful to the two reviewers who helped us to improve the original version of the text.

Conflicts of Interest: The authors declare no conflict of interest.

References

1. Hancock, P.L.; Chalmers, R.M.L.; Altunel, E.; Çakir, Z. Travertines: Using travertines in active fault studies. *J. Struct. Geol.* **1999**, *21*, 903–916. [[CrossRef](#)]
2. Brogi, A.; Alcicek, M.C.; Yalciner, C.C.; Capezzuoli, E.; Liotta, D.; Meccheri, M.; Rimondi, V.; Ruggieri, G.; Gandin, A.; Boschi, C.; et al. Hydrothermal fluids circulation and travertine deposition in an active tectonic setting: Insights from the Kamara geothermal area (western Anatolia, Turkey). *Tectonophysics* **2016**, *680*, 211–232. [[CrossRef](#)]
3. Curewitz, D.; Karson, J.A. Structural settings of hydrothermal outflow: Fracture permeability maintained by fault propagation and interaction. *J. Volcanol. Geotherm. Res.* **1997**, *79*, 149–168. [[CrossRef](#)]
4. Sibson, R.H. Fluid involvement in normal faulting. *J. Geodyn.* **2000**, *29*, 469–499. [[CrossRef](#)]
5. Muir-Wood, R. Neohydrotectonics. *Z. Geomorphol. Suppl.* **1993**, *94*, 275–284.
6. Chafetz, H.S.; Folk, R.L. Travertines; depositional morphology and the bacterially constructed constituents. *J. Sediment. Res.* **1984**, *54*, 289–316. [[CrossRef](#)]
7. Ford, T.D.; Pedley, H.M. A review of tufa and travertine deposits of the world. *Earth-Sci. Rev.* **1996**, *41*, 117–175. [[CrossRef](#)]
8. Bargar, K.E. *Geology and Thermal History of Mammoth Hot Springs, Yellowstone National Park, Wyoming*; US Geological Survey: Washington, DC, USA, 1978; pp. 1–55. [[CrossRef](#)]
9. Altunel, E.; Hancock, P.L. Active fissuring, faulting and travertine deposition at Pamukkale (W Turkey). *Z. Geomorphol. Suppl.* **1993**, *94*, 285–302.
10. Altunel, E.; Hancock, P.L. Morphology and structural setting of Quaternary travertines at Pamukkale, Turkey. *Geol. J.* **1993**, *28*, 335–346. [[CrossRef](#)]
11. Brogi, A.; Capezzuoli, E.; Alcicek, M.C.; Gandin, A. Evolution of a fault-controlled fissure-ridge type travertine deposit in the western Anatolia extensional province: The Cukurbag fissure-ridge (Pamukkale, Turkey). *J. Geol. Soc.* **2014**, *171*, 425–441. [[CrossRef](#)]

12. Mádl-Szőnyi, J.; Tóth, A. Basin-scale conceptual groundwater flow model for an unconfined and confined thick carbonate region. *Hydrogeol. J.* **2015**, *23*, 1359–1380. [[CrossRef](#)]
13. Capezzuoli, E.; Ruggieri, G.; Rimondi, V.; Brogi, A.; Liotta, D.; Alcicek, M.C.; Alcicek, H.; Bulbul, A.; Gandin, A.; Meccheri, M.; et al. Calcite veining and feeding conduits in a hydrothermal system: Insights from a natural section across the Pleistocene Golemezli travertine depositional system (western Anatolia, Turkey). *Sediment. Geol.* **2018**, *364*, 180–203. [[CrossRef](#)]
14. Uysal, I.T.; Feng, Y.; Zhao, J.X.; Altunel, E.; Weatherley, D.; Karabacak, V.; Cengiz, O.; Golding, S.D.; Lawrence, M.G.; Collerson, K.D. U-series dating and geochemical tracing of late Quaternary travertine in co-seismic fissures. *Earth Planet. Sci. Lett.* **2007**, *257*, 450–462. [[CrossRef](#)]
15. Uysal, I.T.; Feng, Y.X.; Zhao, J.X.; Isik, V.; Nuriel, P.; Golding, S.D. Hydrothermal CO₂ degassing in seismically active zones during the late Quaternary. *Chem. Geol.* **2009**, *265*, 442–454. [[CrossRef](#)]
16. Frery, E.; Gratier, J.P.; Ellouz-Zimmerman, N.; Loiselet, C.; Braun, J.; Deschamps, P.; Blamart, D.; Hamelin, B.; Swennen, R. Evolution of fault permeability during episodic fluid circulation: Evidence for the effects of fluid-rock interactions from travertine studies (Utah-USA). *Tectonophysics* **2015**, *651*, 121–137. [[CrossRef](#)]
17. Guido, D.M.; Campbell, K.A. Diverse subaerial and sublacustrine hot spring settings of the Cerro Negro epithermal system (Jurassic, Deseado Massif), Patagonia, Argentina. *J. Volcanol. Geotherm. Res.* **2012**, *229*, 1–12. [[CrossRef](#)]
18. Guido, D.M.; Campbell, K.A. Upper Jurassic travertine at El Macanudo, Argentine Patagonia: A fossil geothermal field modified by hydrothermal silicification and acid overprinting. *Geol. Mag.* **2018**, *155*, 1394–1412. [[CrossRef](#)]
19. Altunel, E.; Hancock, P.L. Structural attributes of travertine-filled extensional fissures in the Pamukkale Plateau, Western Turkey. *Int. Geol. Rev.* **1996**, *38*, 768–777. [[CrossRef](#)]
20. Çakir, Z. Along-strike discontinuity of active normal faults and its influence on Quaternary travertine deposition; Examples from western Turkey. *Turk. J. Earth Sci.* **1999**, *8*, 67–80.
21. Guo, L.; Riding, R. Rapid facies changes in Holocene fissure ridge hot spring travertines, Rapolano Terme, Italy. *Sedimentology* **1999**, *46*, 1145–1158. [[CrossRef](#)]
22. Atabey, E. The formation of fissure ridge type laminated travertine-tufa deposits microscopical characteristics and diagenesis, Kırşehir Central Anatolia. *Bull. Miner. Res. Explor.* **2002**, *123*, 59–65.
23. Altunel, E.; Karabacak, V. Determination of horizontal extension from fissure-ridge travertines: A case study from the Denizli Basin, southwestern Turkey. *Geodin. Acta* **2005**, *18*, 333–342. [[CrossRef](#)]
24. Yanık, G.; Uz, B.; Esenli, F.; Özkul, M.; Yagiz, S.; Jones, B. An example of the fissure-ridge type travertine occurrences: The Cambazli travertine, Turgutlu, west Anatolia. In Proceedings of the 1st International Symposium on Travertine, Denizli, Turkey, 21–25 September 2005; pp. 149–153. [[CrossRef](#)]
25. Mesci, B.L.; Gursoy, H.; Tatar, O. The evolution of travertine masses in the Sivas area (Central Turkey) and their relationships to active tectonics. *Turk. J. Earth Sci.* **2008**, *17*, 219–240.
26. Brogi, A.; Capezzuoli, E. Travertine deposition and faulting: The fault-related travertine fissure-ridge at Terme S. Giovanni, Rapolano Terme (Italy). *Int. J. Earth Sci.* **2009**, *98*, 931–947. [[CrossRef](#)]
27. Selim, H.H.; Yanık, G. Development of the Cambazli (Turgutlu/MANISA) fissure-ridge-type travertine and relationship with active tectonics, Gediz Graben, Turkey. *Quat. Int.* **2009**, *199*, 157–163. [[CrossRef](#)]
28. Temiz, U.; Gokten, E.; Eikenberg, J. U/Th dating of fissure ridge travertines from the Kırşehir region (Central Anatolia Turkey): Structural relations and implications for the Neotectonic development of the Anatolian block. *Geodin. Acta* **2009**, *22*, 201–213. [[CrossRef](#)]
29. Temiz, U.; Eikenberg, J. U/Th dating of the travertine deposited at transfer zone between two normal faults and their neotectonic significance: Cambazli fissure ridge travertines (the Gediz Graben-Turkey). *Geodin. Acta* **2011**, *24*, 95–105. [[CrossRef](#)]
30. De Filippis, L.; Billi, A. Morphotectonics of fissure ridge travertines from geothermal areas of Mammoth Hot Springs (Wyoming) and Bridgeport (California). *Tectonophysics* **2012**, *548*, 34–48. [[CrossRef](#)]
31. De Filippis, L.; Faccenna, C.; Billi, A.; Anzalone, E.; Brilli, M.; Ozkul, M.; Soligo, M.; Tuccimei, P.; Villa, I.M. Growth of fissure ridge travertines from geothermal springs of Denizli Basin, western Turkey. *Geol. Soc. Am. Bull.* **2012**, *124*, 1629–1645. [[CrossRef](#)]
32. De Filippis, L.; Anzalone, E.; Billi, A.; Faccenna, C.; Poncia, P.P.; Sella, P. The origin and growth of a recently-active fissure ridge travertine over a seismic fault, Tivoli, Italy. *Geomorphology* **2013**, *195*, 13–26. [[CrossRef](#)]
33. De Filippis, L.; Faccenna, C.; Billi, A.; Anzalone, E.; Brilli, M.; Soligo, M.; Tuccimei, P. Plateau versus fissure ridge travertines from Quaternary geothermal springs of Italy and Turkey: Interactions and feedbacks between fluid discharge, paleoclimate, and tectonics. *Earth-Sci. Rev.* **2013**, *123*, 35–52. [[CrossRef](#)]
34. Mesci, B.L.; Tatar, O.; Piper, J.D.A.; Gursoy, H.; Altunel, E.; Crowley, S. The efficacy of travertine as a palaeoenvironmental indicator: Palaeomagnetic study of neotectonic examples from Denizli, Turkey. *Turk. J. Earth Sci.* **2013**, *22*, 191–203. [[CrossRef](#)]
35. Berardi, G.; Vignaroli, G.; Billi, A.; Rossetti, F.; Soligo, M.; Kele, S.; Baykara, M.O.; Bernasconi, S.M.; Castorina, F.; Tecce, F.; et al. Growth of a Pleistocene giant carbonate vein and nearby thermogene travertine deposits at Semproniano, southern Tuscany, Italy: Estimate of CO₂ leakage. *Tectonophysics* **2016**, *690*, 219–239. [[CrossRef](#)]
36. Matera, P.F.; Ventruti, G.; Zucchi, M.; Brogi, A.; Capezzuoli, E.; Liotta, D.; Yu, T.L.; Shen, C.C.; Huntington, K.W.; Rinyu, L.; et al. Geothermal Fluid Variation Recorded by Banded Ca-Carbonate Veins in a Fault-Related, Fissure Ridge-Type Travertine Depositional System (Iano, southern Tuscany, Italy). *Geofluids* **2021**, *2021*. [[CrossRef](#)]

37. Mohammadi, Z.; Capezzuoli, E.; Claes, H.; Alipoor, R.; Muchez, P.; Swennen, R. Substrate geology controlling different morphology, sedimentology, diagenesis and geochemistry of adjacent travertine bodies: A case study from the Sanandaj-Sirjan zone (western Iran). *Sediment. Geol.* **2019**, *389*, 127–146. [[CrossRef](#)]
38. Allen, C.C.; Oehler, D.Z. A case for ancient springs in Arabia Terra, Mars. *Astrobiology* **2008**, *8*, 1093–1112. [[CrossRef](#)]
39. Rossi, A.P.; Neukum, G.; Pondrelli, M.; van Gasselt, S.; Zegers, T.; Hauber, E.; Chicarro, A.; Foing, B. Large-scale spring deposits on Mars? *J. Geophys. Res. Planets* **2008**, *113*. [[CrossRef](#)]
40. Pondrelli, M.; Rossi, A.P.; Le Deit, L.; Fueten, F.; van Gasselt, S.; Glamoclija, M.; Cavalazzi, B.; Hauber, E.; Franchi, F.; Pozzobon, R. Equatorial layered deposits in Arabia Terra, Mars: Facies and process variability. *Geol. Soc. Am. Bull.* **2015**, *127*, 1064–1089. [[CrossRef](#)]
41. Pondrelli, M.; Rossi, A.P.; Le Deit, L.; Schmidt, G.; Pozzobon, R.; Hauber, E.; Salese, F. Groundwater Control and Process Variability on the Equatorial Layered Deposits of Kotido Crater, Mars. *J. Geophys. Res. Planets* **2019**, *124*, 779–800. [[CrossRef](#)]
42. Mesci, B.L.; Erkman, A.C.; Gürsoy, H.; Tatar, O. Fossil findings from the Sıcak Çermik fissure ridge-type travertines and possible hominid tracks, Sivas, Central Turkey. *Geodin. Acta* **2018**, *30*, 15–30. [[CrossRef](#)]
43. Gradziński, M.; Bella, P.; Holúbek, P. Constructional caves in freshwater limestone: A review of their origin, classification, significance and global occurrence. *Earth-Sci. Rev.* **2018**, *185*, 179–201. [[CrossRef](#)]
44. Brogi, A. Faults linkage, damage rocks and hydrothermal fluid circulation: Tectonic interpretation of the Rapolano Terme travertines (southern Tuscany, Italy) in the context of Northern Apennines Neogene-Quaternary extension. *Eclogae Geol. Helv.* **2004**, *97*, 307–320. [[CrossRef](#)]
45. Mancini, A.; Frondini, F.; Capezzuoli, E.; Mejia, E.G.; Lezzi, G.; Matarazzi, D.; Brogi, A.; Swennen, R. Evaluating the geogenic CO₂ flux from geothermal areas by analysing quaternary travertine masses. New data from western central Italy and review of previous CO₂ flux data. *Quat. Sci. Rev.* **2019**, *215*, 132–143. [[CrossRef](#)]
46. Jones, B.; Peng, X. Growth and development of spring towers at Shiqiang, Yunnan Province, China. *Sediment. Geol.* **2017**, *347*, 183–209. [[CrossRef](#)]
47. Gao, J.; Zhou, X.; Fang, B.; Li, T.; Tang, L. U-series dating of the travertine depositing near the Rongma hot springs in northern Tibet, China, and its paleoclimatic implication. *Quat. Int.* **2013**, *298*, 98–106. [[CrossRef](#)]
48. Scheuer, G.; Schweitzer, F. Types and forms of travertine cones. *Földtani Közlemény* **1985**, *115*, 385–398, (In Hungarian with English abstract).
49. Liu, Y.P.; Zhou, X.; Fang, B.; Zhou, H.Y.; Yamanaka, T. A preliminary analysis of the formation of travertine and travertine cones in the Jifei hot spring, Yunnan, China. *Environ. Earth Sci.* **2012**, *66*, 1887–1896. [[CrossRef](#)]
50. Atlı, A. The Relationship between Travertine Formations and Regional Tectonics in Hisaralan (Sındırgı) Region. Master's Thesis, Institute of Science and Technology, Balıkesir University, Balıkesir, Turkey, 2018. (In Turkish with English Abstract).
51. Özkul, M.; Gökğöz, A.; Yüksel, A.K. Travertine spring towers as rare depositional morphologies in geothermal fields: An example from the Hisaralan geothermal area (Sındırgı, Balıkesir, NW Turkey). In Proceedings of the International Earth Science Colloquium on the Aegean Region, Izmir, Turkey, 7–11 October 2019.
52. Dekov, V.M.; Egueh, N.M.; Kamenov, G.D.; Bayon, G.; Lalonde, S.V.; Schmidt, M.; Liebetrau, V.; Munnik, F.; Fouquet, Y.; Tanimizu, M.; et al. Hydrothermal carbonate chimneys from a continental rift (Afar Rift): Mineralogy, geochemistry, and mode of formation. *Chem. Geol.* **2014**, *387*, 87–100. [[CrossRef](#)]
53. Pentecost, A. *Travertine*; Springer: Berlin/Heidelberg, Germany, 2005.
54. Jones, B.; Renaut, R.W. Chapter 4 Calcareous spring deposits in continental settings. In *Developments in Sedimentology*; Alonso-Zarza, A.M., Tanner, L.H., Eds.; Elsevier: Amsterdam, The Netherlands, 2010; Volume 61, pp. 177–224.
55. Della Porta, G. Carbonate build-ups in lacustrine, hydrothermal and fluvial settings: Comparing depositional geometry, fabric types and geochemical signature. In *Microbial Carbonates in Space and Time: Implications for Global Exploration and Production*; Bosence, D.W.J., Gibbons, K.A., LeHeron, D.P., Morgan, W.A., Pritchard, T., Vining, B.A., Eds.; Geological Society Special Publication: London, UK, 2015; Volume 418, pp. 17–68.
56. Della Porta, G.; Capezzuoli, E.; De Bernardo, A. Facies character and depositional architecture of hydrothermal travertine slope aprons (Pleistocene, Acquasanta Terme, Central Italy). *Mar. Pet. Geol.* **2017**, *87*, 171–187. [[CrossRef](#)]
57. Gandin, A.; Capezzuoli, E. Travertine: Distinctive depositional fabrics of carbonates from thermal spring systems. *Sedimentology* **2014**, *61*, 264–290. [[CrossRef](#)]
58. Guo, L.; Riding, R. Hot-spring travertine facies and sequences, Late Pleistocene, Rapolano Terme, Italy. *Sedimentology* **1998**, *45*, 163–180. [[CrossRef](#)]
59. Alcicek, M.C.; Alcicek, H.; Altunel, E.; Arenas, C.; Bons, P.; Brogi, A.; Capezzuoli, E.; de Riese, T.; Della Porta, G.; Gandin, A.; et al. Comment on “First records of syn-diagenetic non-tectonic folding in Quaternary thermogene travertines caused by hydrothermal incremental veining” by Billi et al. *Tectonophysics* 700–701 (2017) 60–79. *Tectonophysics* **2017**, *721*, 491–500. [[CrossRef](#)]
60. Gradziński, M.; Wroblewski, W.; Dulinski, M.; Hercman, H. Earthquake-affected development of a travertine ridge. *Sedimentology* **2014**, *61*, 238–263. [[CrossRef](#)]
61. Gradziński, M.; Wróblewski, W.; Holúbek, P. Cenozoic freshwater carbonates of the Central Carpathians (Slovakia): Facies, environments, hydrological control and depositional history. In *Guidebook for Field Trip*; 31st IAS Meeting of Sedimentology, Held in Kraków on 22nd–25th of June 2015; Haczewski, G., Ed.; Polish Geological Society: Krakow, Poland, 2015; Chapter B7; pp. 217–245.

62. Brogi, A.; Capezzuoli, E.; Moretti, M.; Olvera-Garcia, E.; Matera, P.F.; Garduno-Monroy, V.H.; Mancini, A. Earthquake-triggered soft-sediment deformation structures (seismites) in travertine deposits. *Tectonophysics* **2018**, *745*, 349–365. [[CrossRef](#)]
63. De Boever, E.; Brasier, A.T.; Foubert, A.; Kele, S. What do we really know about early diagenesis of non-marine carbonates? *Sediment. Geol.* **2017**, *361*, 25–51. [[CrossRef](#)]
64. Faccenna, C.; Soligo, M.; Billi, A.; De Filippis, L.; Funicello, R.; Rossetti, C.; Tuccimei, P. Late Pleistocene depositional cycles of the Lapis Tiburtinus travertine (Tivoli, Central Italy): Possible influence of climate and fault activity. *Glob. Planet. Chang.* **2008**, *63*, 299–308. [[CrossRef](#)]
65. Karabacak, V.; Uysal, I.T.; Mutlu, H.; Ünal-İmer, E.; Dirik, R.K.; Feng, Y.-X.; Akiska, S.; Aydoğdu, İ.; Zhao, J.-X. Are U-Th dates correlated with historical records of earthquakes? Constraints from coseismic carbonate veins within the North Anatolian Fault Zone. *Tectonics* **2019**, *38*, 2431–2448. [[CrossRef](#)]
66. Kim, Y.S.; Peacock, D.C.P.; Sanderson, D.J. Mesoscale strike-slip faults and damage zones at Marsalforn, Gozo Island, Malta. *J. Struct. Geol.* **2003**, *25*, 793–812. [[CrossRef](#)]
67. Brogi, A.; Capezzuoli, E.; Kele, S.; Baykara, M.O.; Shen, C.C. Key travertine tectofacies for neotectonics and palaeoseismicity reconstruction: Effects of hydrothermal overpressured fluid injection. *J. Geol. Soc.* **2017**, *174*, 679–699. [[CrossRef](#)]
68. Briggs, R.O. Effects of loma prieta earthquake on surface waters in Waddell Valley. *JAWRA J. Am. Water Resour. Assoc.* **1991**, *27*, 991–999. [[CrossRef](#)]
69. Wang, C.Y.; Wang, C.H.; Kuo, C.H. Temporal change in groundwater level following the 1999 (M-W = 7.5) Chi-Chi earthquake, Taiwan. *Geofluids* **2004**, *4*, 210–220. [[CrossRef](#)]
70. Wang, C.Y.; Manga, M. Hydrologic responses to earthquakes and a general metric. *Geofluids* **2010**, *10*, 206–216. [[CrossRef](#)]
71. Lee, M.; Liu, T.K.; Ma, K.F.; Chang, Y.M. Coseismic hydrological changes associated with dislocation of the September 21, 1999 Chichi earthquake, Taiwan. *Geophys. Res. Lett.* **2002**, *29*. [[CrossRef](#)]
72. Brodsky, E.E.; Roeloffs, E.; Woodcock, D.; Gall, I.; Manga, M. A mechanism for sustained groundwater pressure changes induced by distant earthquakes. *J. Geophys. Res.-Solid Earth* **2003**, *108*. [[CrossRef](#)]
73. Elkhoury, J.E.; Brodsky, E.E.; Agnew, D.C. Seismic waves increase permeability. *Nature* **2006**, *441*, 1135–1138. [[CrossRef](#)]
74. Husen, S.; Smith, R.B.; Waite, G.P. Evidence for gas and magmatic sources beneath the Yellowstone volcanic field from seismic tomographic imaging. *J. Volcanol. Geotherm. Res.* **2004**, *131*, 397–410. [[CrossRef](#)]
75. Bonini, M. Mud volcano eruptions and earthquakes in the Northern Apennines and Sicily, Italy. *Tectonophysics* **2009**, *474*, 723–735. [[CrossRef](#)]
76. Manga, M.; Brumm, M.; Rudolph, M.L. Earthquake triggering of mud volcanoes. *Mar. Pet. Geol.* **2009**, *26*, 1785–1798. [[CrossRef](#)]
77. Rudolph, M.L.; Manga, M. Mud volcano response to the 4 April 2010 El Mayor-Cucapah earthquake. *J. Geophys. Res. Solid Earth* **2010**, *115*. [[CrossRef](#)]
78. Wang, C.-Y.; Manga, M.; Dreger, D.; Wong, A. Streamflow increase due to rupturing of hydrothermal reservoirs: Evidence from the 2003 San Simeon, California, Earthquake. *Geophys. Res. Lett.* **2004**, *31*. [[CrossRef](#)]
79. Manga, M.; Brodsky, E. Seismic triggering of eruptions in the far field: Volcanoes and geysers. *Annu. Rev. Earth Planet. Sci.* **2006**, *34*, 263–291. [[CrossRef](#)]
80. Brogi, A.; Capezzuoli, E. Earthquake impact on fissure-ridge type travertine deposition. *Geol. Mag.* **2014**, *151*, 1135–1143. [[CrossRef](#)]
81. Barbier, E. Geothermal energy technology and current status: An overview. *Renew. Sustain. Energy Rev.* **2002**, *6*, 3–65. [[CrossRef](#)]
82. Karabacak, V.; Uysal, I.T.; Ünal-İmer, E.; Mutlu, H.; Zhao, J.X. U-Th age evidence from carbonate veins for episodic crustal deformation of Central Anatolian Volcanic Province. *Quat. Sci. Rev.* **2017**, *177*, 158–172. [[CrossRef](#)]
83. Koban, C.G.; Schweigert, G. Microbial origin of travertine fabrics—Two examples from Southern Germany (Pleistocene stuttgart travertines and miocene riedöschingen Travertine). *Facies* **1993**, *29*, 251–263. [[CrossRef](#)]
84. Flügel, E. *Microfacies of Carbonate Rocks: Analysis, Interpretation and Application*; Springer Science & Business Media: Berlin, Germany, 2004.
85. Temiz, U.; Gokten, Y.E.; Eikenberg, J. Strike-slip deformation and U/Th dating of travertine deposition: Examples from North Anatolian Fault Zone, Bolu and Yenicag Basins, Turkey. *Quat. Int.* **2013**, *312*, 132–140. [[CrossRef](#)]
86. Ronchi, P.; Cruciani, F. Continental carbonates as a hydrocarbon reservoir, an analog case study from the travertine of Saturnia, Italy. *AAPG Bull.* **2015**, *99*, 711–734. [[CrossRef](#)]
87. Brogi, A.; Liotta, D.; Ruggieri, G.; Capezzuoli, E.; Meccheri, M.; Dini, A. An overview on the characteristics of geothermal carbonate reservoirs in southern Tuscany. *Ital. J. Geosci.* **2016**, *135*, 17–29. [[CrossRef](#)]
88. Yildirim, G.; Mutlu, H.; Karabacak, V.; Uysal, I.T.; Dirik, K.; Temel, A.; Yuce, G.; Zhao, J.X. Temporal changes in geochemical-isotopic systematics of the late Pleistocene Akkaya travertines (Turkey)—Implications for fluid flow circulation and seismicity. *Geochemistry* **2020**, *80*. [[CrossRef](#)]
89. Karabacak, V.; Mutlu, H.; Deniz, K. Manifestations of Quaternary syn-eruptive fluid circulations on carbonate veins, Central Anatolian Volcanic Province. *J. Quat. Sci.* **2021**, *36*, 124–137. [[CrossRef](#)]
90. Sibson, R.H. Earthquake rupturing as a mineralizing agent in hydrothermal systems. *Geology* **1987**, *15*, 701–704. [[CrossRef](#)]

91. Nuriel, P.; Rosenbaum, G.; Uysal, T.I.; Zhao, J.; Golding, S.D.; Weinberger, R.; Karabacak, V.; Avni, Y. Formation of fault-related calcite precipitates and their implications for dating fault activity in the East Anatolian and Dead Sea fault zones. In *Geology of the Earthquake Source: A Volume in Honour of Rick Sibson*; Fagereng, A., Toy, V.G., Rowland, J.V., Eds.; Geological Society Special Publication: London, UK, 2011; Volume 359, pp. 229–248.
92. Kampman, N.; Burnside, N.M.; Shipton, Z.K.; Chapman, H.J.; Nicholl, J.A.; Ellam, R.M.; Bickle, M.J. Pulses of carbon dioxide emissions from intracrustal faults following climatic warming. *Nat. Geosci.* **2012**, *5*, 352–358. [[CrossRef](#)]
93. Gratier, J.-P.; Frery, E.; Deschamps, P.; Røyne, A.; Renard, F.; Dysthe, D.; Ellouz-Zimmerman, N.; Hamelin, B. How travertine veins grow from top to bottom and lift the rocks above them: The effect of crystallization force. *Geology* **2012**, *40*, 1015–1018. [[CrossRef](#)]
94. Rimondi, V.; Costagliola, P.; Ruggieri, G.; Benvenuti, M.; Boschi, C.; Brogi, A.; Capezzuoli, E.; Morelli, G.; Gasparon, M.; Liotta, D. Investigating fossil hydrothermal systems by means of fluid inclusions and stable isotopes in banded travertine: An example from Castelnuovo dell’Abate (southern Tuscany, Italy). *Int. J. Earth Sci.* **2016**, *105*, 659–679. [[CrossRef](#)]
95. Vignaroli, G.; Berardi, G.; Billi, A.; Kele, S.; Rossetti, F.; Soligo, M.; Bernasconi, S.M. Tectonics, hydrothermalism, and paleoclimate recorded by Quaternary travertines and their spatio-temporal distribution in the Albegna basin, central Italy: Insights on Tyrrhenian margin neotectonics. *Lithosphere* **2016**, *8*, 335–358. [[CrossRef](#)]
96. Chafetz, H.S.; Akdim, B.; Julia, R.; Reid, A. Mn- and Fe-rich black travertine shrubs: Bacterially (and nanobacterially) induced precipitates. *J. Sediment. Res.* **1998**, *68*, 404–412. [[CrossRef](#)]
97. Chafetz, H.S.; Guidry, S.A. Bacterial shrubs, crystal shrubs, and ray-crystal shrubs: Bacterial vs. abiotic precipitation. *Sediment. Geol.* **1999**, *126*, 57–74. [[CrossRef](#)]
98. Vettori, S.; Cantisani, E.; Chelazzi, L.; Cuzman, O.A.; Gatta, G.D.; D’Andria, F. The dark colour of the Ploutonion at Hierapolis of Phrygiae (Turkey). *Archaeometry* **2019**, *61*, 296–308. [[CrossRef](#)]
99. Pichler, T.; Veizer, J. The precipitation of aragonite from shallow-water hydrothermal fluids in a coral reef, Tutum Bay, Ambitle Island, Papua New Guinea. *Chem. Geol.* **2004**, *207*, 31–45. [[CrossRef](#)]
100. Williams, R.T.; Goodwin, L.B.; Sharp, W.D.; Mozley, P.S. Reading a 400,000-year record of earthquake frequency for an intraplate fault. *Proc. Natl. Acad. Sci. USA* **2017**, *114*, 4893–4898. [[CrossRef](#)]
101. Uysal, I.T.; Feng, Y.X.; Zhao, J.X.; Bolhar, R.; Isik, V.; Baublys, K.A.; Yago, A.; Golding, S.D. Seismic cycles recorded in late Quaternary calcite veins: Geochronological, geochemical and microstructural evidence. *Earth Planet. Sci. Lett.* **2011**, *303*, 84–96. [[CrossRef](#)]
102. Lippmann, F. *Sedimentary Carbonate Minerals*, 07/05 ed.; Springer: Berlin/Heidelberg, Germany; New York, NY, USA, 1973.
103. Folk, R.L. Interaction between bacteria, nannobacteria, and mineral precipitation in hot-springs of central Italy. *Geogr. Phys. Quat.* **1994**, *48*, 233–246. [[CrossRef](#)]
104. Fouke, B.W.; Farmer, J.D.; Des Marais, D.J.; Pratt, L.; Sturchio, N.C.; Burns, P.C.; Discipulo, M.K. Depositional facies and aqueous-solid geochemistry of travertine-depositing hot springs (Angel Terrace, Mammoth Hot Springs, Yellowstone National Park, USA). *J. Sediment. Res.* **2000**, *70*, 565–585. [[CrossRef](#)]
105. Lippmann, F. Versuche zur Aufklärung der Bildungsbedingungen von Calcit und Aragonit. *Fortschr. Mineral.* **1960**, *38*, 156–161. (In German)
106. Flinn, D.; Pentecost, A. Travertine-cemented screes on the serpentinite seacliffs of Unst and Fetlar, Shetland. *Mineral. Mag.* **1995**, *59*, 259–265. [[CrossRef](#)]
107. Malesani, P.; Vannucci, S. Precipitazione de calcite o di aragonite dale acque termominerali in relazione alla genesi e all’evoluzione dei travertine. *Atti Accad. Naz. Lincei Cl. Sci. Fis. Mat. Nat. Rend.* **1975**, *58*, 761–776. (In Italian)
108. Duchi, V. Riesame del problema della precipitazione di calcite od aragonite da soluzioni naturali. *Rendiconti* **1978**, *34*, 605–618. (In Italian)
109. Rankama, K.; Sahama, T.G. *Geochemistry*; University of Chicago Press: Chicago, IL, USA, 1950.
110. Uysal, I.T.; Unal-Imer, E.; Shulmeister, J.; Zhao, J.X.; Karabacak, V.; Feng, Y.X.; Bolhar, R. Linking CO₂ degassing in active fault zones to long-term changes in water balance and surface water circulation, an example from SW Turkey. *Quat. Sci. Rev.* **2019**, *214*, 164–177. [[CrossRef](#)]
111. Ricketts, J.W.; Ma, L.; Wagler, A.E.; Garcia, V.H. Global travertine deposition modulated by oscillations in climate. *J. Quat. Sci.* **2019**. [[CrossRef](#)]
112. Brogi, A.; Capezzuoli, E.; Aqué, R.; Branca, M.; Voltaggio, M. Studying travertines for neotectonics investigations: Middle–Late Pleistocene syn-tectonic travertine deposition at Serre di Rapolano (Northern Apennines, Italy). *Int. J. Earth Sci.* **2010**, *99*, 1383–1398. [[CrossRef](#)]
113. Guo, L.; Riding, R. Aragonite laminae in hot water travertine crusts, Rapolano Terme, Italy. *Sedimentology* **1992**, *39*, 1067–1079. [[CrossRef](#)]
114. Carrara, C.; Ciuffarella, L.; Paganin, G. Inquadramento geomorfologico e climatico-ambientale dei travertini di Rapolano Terme (SI). *Ital. J. Quat. Sci.* **1998**, *11*, 319–329.
115. Pedley, M. Tufas and travertines of the Mediterranean region: A testing ground for freshwater carbonate concepts and developments. *Sedimentology* **2009**, *56*, 221–246. [[CrossRef](#)]
116. Brogi, A.; Liotta, D.; Capezzuoli, E.; Matera, P.F.; Kele, S.; Soligo, M.; Tuccimei, P.; Ruggieri, G.; Yu, T.L.; Shen, C.C.; et al. Travertine deposits constraining transfer zone neotectonics in geothermal areas: An example from the inner Northern Apennines (Bagno Vignoni-Val d’Orcia area, Italy). *Geothermics* **2020**, *85*. [[CrossRef](#)]

117. Altunel, E. *Active Tectonics and the Evolution of Quaternary Travertines at Pamukkale, Western Turkey*; University of Bristol: Bristol, UK, 1994.
118. Yalçiner, C.Ç. Investigation of the subsurface geometry of fissure-ridge travertine with GPR, Pamukkale, western Turkey. *J. Geophys. Eng.* **2013**, *10*. [[CrossRef](#)]
119. Brogi, A.; Alcicek, M.C.; Liotta, D.; Capezzuoli, E.; Zucchi, M.; Matera, P.F. Step-over fault zones controlling geothermal fluid-flow and travertine formation (Denizli Basin, Turkey). *Geothermics* **2021**, *89*. [[CrossRef](#)]
120. Koen, V.N.; Claes, H.; Soete, J.; Foubert, A.; Özkul, M.; Swennen, R. Fracture networks and strike-slip deformation along reactivated normal faults in Quaternary travertine deposits, Denizli Basin, western Turkey. *Tectonophysics* **2013**, *588*, 154–170. [[CrossRef](#)]
121. Sağlam Selçuk, A.; Erturaç, M.K.; Üner, S.; Özsayin, E.; Pons-Branchu, E. Evolution of Camlik fissure-ridge travertines in the Baskale basin (Van, Eastern Anatolia). *Geodin. Acta* **2017**, *29*, 1–19. [[CrossRef](#)]
122. Temiz, U.; Savaş, F. Relationship between Akhüyük fissure ridge travertines and active tectonics: Their neotectonic significance (Ereğli-Konya, Central Anatolia). *Arab. J. Geosci.* **2015**, *8*, 2383–2392. [[CrossRef](#)]
123. Mesci, B.L. Active tectonics of the Ortakoy fissure-ridge-type travertines: Implications for the Quaternary stress state of the neotectonic structures of the Central Anatolia, Turkey. *Geodin. Acta* **2012**, *25*, 12–25. [[CrossRef](#)]
124. Karabacak, V.; Ring, U.; Uysal, I.T. The off-fault deformation on the North Anatolian Fault zone and assessment of slip rate from carbonate veins. *Tectonophysics* **2020**, *795*, 228633. [[CrossRef](#)]
125. Mesci, B.L.; GURSOY, H.; Ghaleb, B.; Tatar, O. An extensional fracture acting as hot water source for travertine deposition on the North Anatolian Fault Zone, Turkey: The Resadiye Fissure-Ridge. *Turk. Jeol. Bul. Geol.* **2020**, *63*, 145–160. [[CrossRef](#)]
126. Tekin, E.; Kayabali, K.; Ayyidiz, T.; Ileri, O. Evidence of microbiologic activity in modern travertines: Sicakcermik geothermal field, central Turkey. *Carbonates Evaporites* **2000**, *15*, 18–27. [[CrossRef](#)]
127. Çolak Erol, S.; Özkul, M.; Aksoy, E.; Kele, S.; Ghaleb, B. Travertine occurrences along major strike-slip fault zones: Structural, depositional and geochemical constraints from the Eastern Anatolian Fault System (EAFS), Turkey. *Geodin. Acta* **2015**, *27*, 155–174. [[CrossRef](#)]
128. Kalender, L.; Okan, O.O.; Inceoz, M.; Cetindag, B.; Yildirim, V. Geochemistry of travertine deposits in the Eastern Anatolia District: An example of the Karakocan-Yogunagac (Elazig) and Mazgirt-Dedebag (Tunceli) travertines, Turkey. *Turk. J. Earth Sci.* **2015**, *24*, 607–626. [[CrossRef](#)]
129. Karabacak, V. General properties of Ihlara Valley (central Anatolia) travertines and their implications on crustal deformation. *J. Eng. Archit. Fac. Eskişehir Osman. Univ.* **2007**, *20*, 65–82. [[CrossRef](#)]
130. Temiz, U.; Koçak, İ.; Öksüz, N.; Akbay, S. U-series dating and origin of Yaprakhisar (Guzelyurt-Aksaray) travertines in Central Anatolian Volcanic Province, Turkey. *Arab. J. Geosci.* **2018**, *11*. [[CrossRef](#)]
131. Temiz, U.; Savaş, F. U/Th Dating of the Akhuyuk Fissure Ridge Travertines in Ereğli, Konya (Central Anatolia, Turkey): Their Relationship to Active Tectonics. *Arab. J. Sci. Eng.* **2018**, *43*, 3739–3749. [[CrossRef](#)]
132. Rizzo, A.; Uysal, I.T.; Mutlu, H.; Unal-Imer, E.; Dirik, K.; Yuce, G.; Caracausi, A.; Misseri, M.; Temel, A.; Bayari, S.; et al. Geochemistry of fluid inclusions in travertines from Western and Northern Turkey: Inferences on the role of active faults in fluids circulation. *Geochem. Geophys. Geosystems* **2019**. [[CrossRef](#)]
133. Ricketts, J.W.; Karlstrom, K.E.; Prewisch, A.; Crossey, L.J.; Polyak, V.J.; Asmerom, Y. Quaternary extension in the Rio Grande rift at elevated strain rates recorded in travertine deposits, central New Mexico. *Lithosphere* **2014**, *6*, 3–16. [[CrossRef](#)]
134. Török, Á.; Claes, H.; Brogi, A.; Liotta, D.; Tóth, Á.; Mindszenty, A.; Kudó, I.; Kele, S.; Shen, C.-C.; Rudy, S. A multi-methodological approach to reconstruct the configuration of a travertine fissure ridge system: The case of the Cukor quarry (Süttő, Gerecse Hills, Hungary). *Geomorphology* **2019**, *345*. [[CrossRef](#)]
135. Kele, S.; Korpás, L.; Demény, A.; Kovács-Pálffy, P.; Bajnóczi, B.; Medzihradzsky, Z. Paleoenvironmental evaluation of the Tata Travertine Complex (Hungary), based on stable isotopic and petrographic studies. *Acta Geol. Hung.* **2006**, *49*, 1–31. [[CrossRef](#)]
136. HENCHIRI, M.; Ben Ahmed, W.; Brogi, A.; Alcicek, M.C.; Benassi, R. Evolution of Pleistocene travertine depositional system from terraced slope to fissure-ridge in a mixed travertine-alluvial succession (Jebel El Mida, Gafsa, southern Tunisia). *Geodin. Acta* **2017**, *29*, 20–41. [[CrossRef](#)]
137. Rahmani Javanmard, S.; Tutti, F.; Omidian, S.; Ranjbaran, M. Mineralogy and stable isotope geochemistry of the Ab Ask travertines in Damavand geothermal field, Northeast Tehran, Iran. *Cent. Eur. Geol.* **2012**, *55*, 187–212. [[CrossRef](#)]
138. Rahmani Javanmard, S.; Tutti, F.; Omidian, S.; Ranjbaran, M. Mineralogy and the genesis of fissure-ridge and vein type travertine (in Ab-E Ask) based on petrographic studies and carbon and oxygen isotopes analysis. *Iran. J. Geol.* **2012**, *6*, 51–61.
139. Ranjbaran, M.; Rahmani Javanmard, S. Petrography and geochemistry of Quaternary travertines in the Ab-e Ask region, Mazandaran Province- Iran. *Geopersia* **2019**, *9*, 351–365. [[CrossRef](#)]
140. Mohajjel, M.; Taghipour, K. Quaternary travertine ridges in the Lake Urmia area: Active extension in NW Iran. *Turk. J. Earth Sci.* **2014**, *23*, 602–614. [[CrossRef](#)]
141. Roshanak, R.; Moore, F.; ZARASVANDI, A.; Keshavarzi, B.; Gratzner, R. Stable isotope geochemistry and petrography of the Qorveh-Takab travertines in northwest Iran. *Austrian J. Earth Sci.* **2018**, *111*, 64–74. [[CrossRef](#)]
142. Ghazi, J.M.; Olafsdottir, R.; Tongkul, F.; Ghazi, J.M. Geological Features for Geotourism in the Western Part of Sahand Volcano, NW Iran. *Geoheritage* **2013**, *5*, 23–34. [[CrossRef](#)]

143. Echeveste, H. Travertines and jasperoids of the Manantial Espejo, a Jurassic hot spring environment. Macizo del Deseado, Santa Cruz Province, Argentina. *Lat. Am. J. Sedimentol. Basin Anal.* **2005**, *12*, 33–48. (In Spanish)
144. Renaut, R.W.; Morley, C.K.; Jones, B.; Renaut, R.W.; Ashley, G.M. Fossil hot-spring travertine in the Turkana Basin, Northern Kenya: Structure, facies, and genesis. In *Sedimentation in Continental Rifts*; SEPM Society for Sedimentary Geology: Broken Arrow, OK, USA, 2002; Volume 73.
145. Quade, J.; Rasbury, E.T.; Huntington, K.; Hudson, A.; Vonhof, H.; Anchukaitis, K.; Betancourt, J.; Latorre, C.; Pepper, M. Isotopic characterization of late Neogene travertine deposits at Barrancas Blancas in the eastern Atacama Desert, Chile. *Chem. Geol.* **2017**, *466*, 41–56. [[CrossRef](#)]
146. Salminen, P.E.; Brasier, A.T.; Karhu, J.A.; Melezhik, V.A. Travertine precipitation in the Paleoproterozoic Kuetsjarvi Sedimentary Formation, Pechenga Greenstone Belt, NE Fennoscandian Shield. *Precambrian Res.* **2014**, *255*, 181–201. [[CrossRef](#)]
147. Ufrecht, W.; Kluge, T. Die Travertine von Böttingen und Laichingen (Miozän, mittlere Schwäbische Alb)–Archive für ein Paläo-Thermalwassersystem. *Z. Dtsch. Ges. Geowiss.* **2020**, *2020*, 365–389, (In German with English abstract).
148. Shiraishi, F.; Morikawa, A.; Kuroshima, K.; Amekawa, S.; Yu, T.L.; Shen, C.C.; Kakizaki, Y.; Kano, A.; Asada, J.; Bahniuk, A.M. Genesis and diagenesis of travertine, Futamata hot spring, Japan. *Sediment. Geol.* **2020**, *405*. [[CrossRef](#)]
149. Akdim, B.; Julia, R.A. The travertine mounds of Tafilalet (Morocco): Morphology and genesis based on present-day analogues. *Z. Geomorphol.* **2005**, *49*, 373–389.
150. Kampman, N.; Bickle, M.; Galy, A.; Chapman, H.; Zhou, Z.; Dubacq, B.; Wigley, M.; Warr, O.; Sirikitputtisak, T.; Ballentine, C. Short-term CO₂–fluid–mineral interactions in a CO₂ injection experiment, Wyoming. *Mineral. Mag.* **2011**, *75*, 1149.
151. El Desouky, H.; Soete, J.; Claes, H.; Ozkul, M.; Vanhaecke, F.; Swennen, R. Novel applications of fluid inclusions and isotope geochemistry in unravelling the genesis of fossil travertine systems. *Sedimentology* **2015**, *62*, 27–56. [[CrossRef](#)]
152. Gibert, R.O.; Taberner, C.; Saez, A.; Giralt, S.; Alonso, R.N.; Edwards, R.L.; Pueyo, J.J. Igneous origin of CO₂ in ancient and recent hot-spring waters and travertines from the northern Argentinean Andes. *J. Sediment. Res.* **2009**, *79*, 554–567. [[CrossRef](#)]
153. Janssens, N.; Capezzuoli, E.; Claes, H.; Muchez, P.; Yu, T.L.; Shen, C.C.; Ellam, R.M.; Swennen, R. Fossil travertine system and its palaeofluid provenance, migration and evolution through time: Example from the geothermal area of Acquasanta Terme (Central Italy). *Sediment. Geol.* **2020**, *398*. [[CrossRef](#)]
154. Słowakiewicz, M. Fluid inclusion data in calcite from the Upper Triassic hot-spring travertines in southern Poland. *J. Geochem. Explor.* **2003**, *78–79*, 123–126. [[CrossRef](#)]